

# Higgs-strahlung at the LHC in the inert doublet model

Dazhuang He<sup>\*</sup>,<sup>1</sup> Yu Zhang<sup>†,2</sup> Boudjema Fawzi<sup>‡,3</sup> and Hao Sun<sup>§1</sup>

<sup>1</sup>*Institute of Theoretical Physics, School of Physics, Dalian University of Technology,  
No.2 Linggong Road, Dalian, Liaoning, 116024, P.R.China*

<sup>2</sup>*School of Physics, Hefei University of Technology, Hefei 230601, China*

<sup>3</sup>*LAPTh, Université Savoie Mont Blanc, CNRS, BP 110, F-74000 Annecy, France*

(Dated: Tuesday 20<sup>th</sup> February, 2024)

$pp \rightarrow W^\pm h, Zh$  processes at the LHC are studied in the framework of the inert doublet model (IDM). To quantify the effects of the IDM and their observability in these processes we revisit the NLO (QCD and EW) predictions in the Standard Model (SM) and their uncertainty. Taking all available current constraints on the parameter space of the IDM, we consider both the case of the IDM providing a good Dark Matter (DM) candidate within the freeze-out mechanism as well as when the DM restrictions are relaxed. In the former, deviations from the SM of only a few per-mil in these cross sections at the LHC are found and may not be measured. In the latter, the deviations can reach a few percents and should be observable. Smaller discrepancies in this case require theoretical uncertainties to be improved in particular those arising from the parton distribution functions (PDFs). We stress the importance of the photon induced real corrections and the need for further improvement in the extraction of the photon PDFs. The analysis also showcases the development and exploitation of our automated tool for the computation of one-loop electroweak and QCD corrections for a New Physics model with internal tests such as those concerning the soft and collinear parts provided through both dipole subtraction and phase space slicing besides tests for ultra-violet finiteness and gauge-parameter independence.

## Contents

<b>I. Introduction</b>	<b>2</b>
<b>II. The Inert Higgs Doublet Model, description and constraints</b>	<b>3</b>
A. A brief description to IDM	3
B. The current constraints	4
1. Theoretical constraints	4
2. Experimental constraints	5
<b>III. Higgs-strahlung in the SM: QCD and EW 1-loop corrections</b>	<b>8</b>
A. A recap of precision calculations in the SM for $Vh$ processes at the LHC	8
B. Our general approach to NLO QCD and electroweak corrections	8
C. Standard Model Parameters	10
D. Leading Order, LO	10
E. NLO QCD corrections	11
1. Virtual QCD corrections and the corresponding bremsstrahlung real corrections	11
2. Real corrections: $gq$ induced contributions	12
3. $gg$ induced contributions: $Zh$ production	13
4. Comparison with Madgraph for the NLO QCD corrections in the SM.	13
5. Scale and PDFs uncertainty.	14
F. EW corrections in the SM	15
1. Renormalization. The $G_\mu$ scheme	15
2. Virtual one-loop electroweak corrections	16
3. Real photonic corrections for $q\bar{q}$ annihilation	17

<sup>\*</sup> dzhe@mail.dlut.edu.cn

<sup>†</sup> dayu@hfut.edu.cn

<sup>‡</sup> boudjema@lapth.cnrs.fr

<sup>§</sup> haosun@dlut.edu.cn

4. Combining (photonic) real and virtual corrections soft/collinear divergences	17
5. $q\gamma$ initiated annihilation	18
6. $\gamma\gamma$ induced $Zh$ production in the SM	19
7. Results, Scale dependence and PDFs uncertainty of the electroweak corrections in the SM. Impact on the full NLO corrections	19
G. Electroweak and QCD NLO corrections in the SM	21
<b>IV. Higgs-strahlung in the IDM: One loop results and deviations from the SM</b>	<b>22</b>
A. Scenarios without DM constraints	23
B. Scenarios with DM constraints	28
<b>V. Summary</b>	<b>28</b>
<b>Acknowledgments</b>	<b>28</b>
<b>References</b>	<b>29</b>

## I. INTRODUCTION

The discovery of the Higgs boson [1, 2] at the Large Hadron Collider (LHC) in 2012 was the crowning of the Standard Model (SM) and vindication of mass generation through the mechanism of electroweak symmetry breaking. There is some unease with the rather light mass of the Higgs boson,  $M_h = 125$  GeV, compared to, for example, the large scales derived from the indirect effect the New Physics in flavour observables. Yet, Higgs observables can now be used to probe the structure of electroweak symmetry breaking. One approach is a model independent approach in the context of effective operators and their effects on a large set of observables, not necessarily Higgs related. The other approach is within a coherent UV completion, *i.e.* a fully fledged model. If the model is unitary and renormalisable, a programme based on precision calculations can be conducted. This programme includes direct searches for, in principle, the particle content of the model but also the indirect effects of these particles, and modified couplings, in standard model processes. One aim of this paper is to concentrate on the indirect effects. Considering that the SM has passed so many tests with flying colours one can ask whether any extension is already so constrained through existing observables now that prospects for seeing any deviation as a sign of New Physics (NP) in the future, in particular at the LHC, are slim. To be able to return a sound answer a better determination of the theoretical uncertainties in SM predictions is in order, as well as more precise experimental measurements. In the approach based on a well defined model, it is best to first start these investigations with a rather simplified, UV complete, model. The Inert Doublet Model, IDM [3–5], is one such model. It is a simplified two Higgs Doublet Model (2HDM) containing only an extra Higgs doublet to the SM. The IDM has a rich phenomenology both at the colliders and in Dark Matter (DM) physics, and as such has been widely studied [6–75] mostly in tree-level analyses but also including higher order corrections, either electroweak (EW) or QCD.

In this paper we quantify the *indirect* impact of the IDM on the Higgs-strahlung,  $pp \rightarrow Vh, V = W^\pm, Z$  cross sections and distributions at the LHC once the current constraints on the model (theoretical considerations, precision electroweak observables, non observation of the heavy scalars, Higgs decays) are imposed. If the IDM is to qualify as a model of DM, we study the additional constraints set by DM observables, in particular the relic density and direct detection. The indirect effects of the IDM in Higgs-strahlung processes necessarily involve one-loop corrections which, for the IDM, take place in the electroweak sector. Nonetheless the issue of the SM theoretical uncertainties arises, these are both of QCD and electroweak nature in the context of the LHC. The other aim of this paper is to showcase the improvements made in an automatic one loop calculator that performs both QCD and electroweak corrections and that handles both the SM and a new physics model (IDM in this case) beyond leading order. In this respect we go through the different elements (QCD and EW) that build up the SM and IDM contributions to the Higgs-strahlung beyond tree-level.

The structure of this paper is as follows. In section II we briefly describe the Lagrangian of the IDM and underline the set of physical parameters necessary to define the model. By closely following the extensive study we performed in [64] we update the allowed parameter space (theoretical considerations and current experimental constraints) on the parameter space of the model. We classify models within two categories, those where the IDM does not provide a DM candidate but pass all other constraints and those more constrained models where the IDM furnishes a DM candidate. Within each category we propose some benchmark points. In section III, the LO and NLO, QCD and electroweak, calculations for Higgs-strahlung are discussed and their implementation in our code addressed.

Since these processes at the LHC set an example to upcoming automation of NLO processes, with both QCD and EW corrections, we go through the generation of the virtual and the different parts of the real (bremsstrahlung,  $gq/\gamma q$  and  $gg/\gamma\gamma$  induced) corrections. Tuned comparisons for the QCD NLO corrections with MadGraph[76] are performed and found to be excellent. For the electroweak corrections we use an OS (on-shell scheme) but contrary to many of our previous studies (SloopS [55, 77–84]) we use the so-called  $\alpha_{G_\mu}$  scheme instead of the fine structure constant defined from Compton scattering. This merges well with the QCD corrections and allows the use of massless fermions. Also, new compared to our previous studies of NLO corrections, in handling the infrared/collinear divergences, we use both the dipole subtraction[85–87] and the two-cutoff phase space slicing methods [88]. This serves as an additional check for our calculations both in QCD in the EW corrections. We underline the importance of the photon induced corrections and the need for a good determination of the photon PDFs. Section IV is devoted to the generation of the one-loop extra corrections within the IDM. Results for the IDM contribution on the inclusive cross sections for a large scan on the allowed parameter space are presented. We also study, for some benchmark points, the effects on the transverse momentum and rapidity of the Higgs. We wrap up with a concise summary in section V.

## II. THE INERT HIGGS DOUBLET MODEL, DESCRIPTION AND CONSTRAINTS

### A. A brief description to IDM

The IDM is a 2 Higgs Doublet Model (2HDM). Beside the SM scalar doublet  $\Phi_1$  it includes a second scalar doublet,  $\Phi_2$ , which does not take part in electroweak symmetry breaking. A discrete  $\mathbb{Z}_2$  symmetry is built in whereby all the SM fields are even, such that under this symmetry transformation  $\Phi_1 \rightarrow \Phi_1$ , whereas the new scalars are odd  $\Phi_2 \rightarrow -\Phi_2$ . This symmetry prevents the new scalars to couple to the fermions of the SM through renormalisable operators. It also restricts the form of the (renormalisable) Lagrangian, in particular the extended scalar potential.

Following the notations we gave in Ref. [64], the IDM Lagrangian is

$$\mathcal{L}_{\text{IDM}}^{\text{scalar}} = (D^\mu \Phi_1)^\dagger D_\mu \Phi_1 + (D^\mu \Phi_2)^\dagger D_\mu \Phi_2 - V_{\text{IDM}}(\Phi_1, \Phi_2), \quad (1)$$

with the scalar potential

$$\begin{aligned} V_{\text{IDM}}(\Phi_1, \Phi_2) = & \mu_1^2 |\Phi_1|^2 + \mu_2^2 |\Phi_2|^2 + \lambda_1 |\Phi_1|^4 + \lambda_2 |\Phi_2|^4 + \lambda_3 |\Phi_1|^2 |\Phi_2|^2 + \lambda_4 |\Phi_1^\dagger \Phi_2|^2 \\ & + \frac{1}{2} \lambda_5 \left( (\Phi_1^\dagger \Phi_2)^2 + \text{h.c.} \right), \end{aligned} \quad (2)$$

where the parameters  $\mu_i$  and  $\lambda_i$  are real valued and  $D_\mu$  is the covariant derivative. We parameterise the Higgs doublets as

$$\Phi_1 = \begin{pmatrix} G^+ \\ \frac{1}{\sqrt{2}}(v + h + iG^0) \end{pmatrix} \quad \text{and} \quad \Phi_2 = \begin{pmatrix} H^+ \\ \frac{1}{\sqrt{2}}(X + iA) \end{pmatrix}. \quad (3)$$

$G^0$  and  $G^\pm$  are the neutral and charged Goldstone bosons, respectively.  $v$  is the usual vev of the SM with  $v \simeq 246$  GeV. The mass of the  $W$  boson is  $M_W = gv/2$ ,  $g$  is the  $SU(2)$  gauge coupling which relates to the electromagnetic coupling,  $e$  as  $g = e/s_W$ . With  $M_Z$  the mass of the  $Z$  boson,  $M_W^2/M_Z^2 = 1 - s_W^2$  defines  $s_W$ .

The model has five physical mass eigenstates: together with the CP-even SM Higgs  $h$  (with mass  $M_h = 125$  GeV) there are two extra neutral scalars,  $X$  and  $A$ , and a pair of charged scalars  $H^\pm$ . Depending on the masses of  $X$  and  $A$ , both are possible DM candidates, nonetheless, the physics is the same through the interchange  $(\lambda_5, X) \leftrightarrow (-\lambda_5, A)$ . We will consider the scalar  $X$  as the lightest (hence stable) extra neutral scalar,  $M_X < M_A$ . With the minimisation condition on the potential, the scalar masses can be used to define 4 of the parameters of the scalar potential Eqs. 2,3

$$\begin{aligned} M_h^2 &= 3v^3 \lambda_1 + \mu_1^2 = -2\mu_1^2 = 2\lambda_1 v^2, \\ M_{H^\pm}^2 &= \mu_2^2 + \frac{v^2 \lambda_3}{2}, \\ M_X^2 &= \mu_2^2 + \frac{v^2 \lambda_L}{2} = M_{H^\pm}^2 + (\lambda_3 + \lambda_5) \frac{v^2}{2}, \\ M_A^2 &= \mu_2^2 + \frac{v^2 \lambda_A}{2} = M_{H^\pm}^2 + (\lambda_4 - \lambda_5) \frac{v^2}{2} = M_X^2 - \lambda_5 v^2. \end{aligned} \quad (4)$$

The couplings of the SM Higgs to the new scalars can be used as input physical parameters to re-express one of the independent combinations of parameters of the potential

$$\lambda_{L/A} = \lambda_3 + \lambda_4 \pm \lambda_5. \quad (5)$$

For example the coupling of the SM Higgs  $h$  to a pair of lightest neutral scalar  $X$  is

$$\mathcal{A}_{hXX} = -\lambda_L v \quad (\text{the quartic coupling } hhXX \propto \lambda_L). \quad (6)$$

Similarly  $h(h)AA \propto \lambda_A$ ,  $h(h)H^+H^- \propto \lambda_3$ , observe that  $\mu_2$  will be a redundant parameter when  $\lambda_L$  is chosen as an input parameter, as we will do.

There remains one independent parameter to define.  $\lambda_2$  which describes the four-point self-interaction within  $\Phi_2$  makes this couplings totally elusive when we only consider (at tree-level) interaction of any SM particle. For  $W^\pm/Zh$  production at the LHC we are totally insensitive to this parameter,  $\lambda_2$ . In turn we can reconstruct the parameters of the scalar potential though the physical parameters

$$\begin{aligned} \lambda_1 &= \frac{M_h^2}{2v^2}, \\ \lambda_5 &= \frac{M_X^2 - M_A^2}{v^2}, \\ \lambda_4 &= \lambda_5 + 2 \frac{M_A^2 - M_{H^\pm}^2}{v^2}, \\ \lambda_3 &= \lambda_L - \lambda_4 - \lambda_5, \\ \mu_2^2 &= M_X^2 - \lambda_L \frac{v^2}{2} \rightarrow \lambda_L = \frac{2(M_X^2 - \mu_2^2)}{v^2}. \end{aligned} \quad (7)$$

To sum up, besides the input parameters of SM, we will take the set

$$\{M_X, M_A, M_{H^\pm}, \lambda_L, (\lambda_2)\}, \quad (8)$$

as the set of independent input (physical) parameters of the IDM.

Observe that in the limit of mass degeneracy between the three additional scalars,  $M_S = M_X = M_A = M_{H^\pm}$ , we have  $\lambda_4 = \lambda_5 = 0$  and therefore the Higgs has the same coupling to  $X, A$  and  $H^\pm$  with  $\lambda_L = \lambda_3 = \lambda_A$ . When only  $M_A = M_{H^\pm}$ ,  $\lambda_4 = \lambda_5$  and hence  $\lambda_A = \lambda_3$  but  $\lambda_L = \lambda_3 + 2\lambda_4$ . In this case we write  $\Delta M = M_A - M_X > 0$  then with masses in units of GeV  $\lambda_A \sim \lambda_L + \frac{1}{3}(\Delta M/100)((\Delta M/100) + 2(M_X/100)) \sim \lambda_L + 1$  for  $M_X = \Delta M = 100$  GeV.  $\lambda_A$  increases with increasing  $M_X$  and increasing  $\Delta M$ . These remarks are useful when we try to understand the deviations from the SM in loop observables. Exchange of heavy scalars would decouple but heavy scalars can make couplings large.

It is important to keep in mind that, at tree-level, the Higgs-strahlung processes ( $pp \rightarrow W^\pm h, Zh$ ) we are about to study do not depend on the set of parameters introduced by the new scalars and therefore these processes give exactly the same value for these cross sections at tree-level as in the SM. The NLO QCD corrections are also the same as in the SM, differences appear in the electroweak NLO corrections.

## B. The current constraints

The IDM parameters space (Eq. 8) is already quite constrained. We have already performed a detailed thorough investigation of these constraints in [64]. Here we will update the constraints taking into account recent data from key observables. We first redelimit the constraints without assuming that the IDM provides a model of DM. In a second stage we take the IDM to provide a good DM candidate and derive the more restrictive allowed parameter space.

### 1. Theoretical constraints

These concern theoretical arguments based on perturbativity, vacuum stability, unitarity and charge breaking-minima. We bring no change to the analysis we made in [64], see also [89, 90]

## 2. Experimental constraints

### 1): Electroweak Precision Observables (EWPO).

Through the  $S$ ,  $T$ ,  $U$  parameters [91], these relate to the two-point functions of the vector bosons as inferred from precision measurements of  $Z$  observables. Some of these two-point functions,  $\pi_{AB}(Q^2)$  (for a  $A \rightarrow B$  transition),  $Q^2 \neq M_W^2, M_Z^2$  will appear in the one-loop corrections to  $pp \rightarrow Vh$ . In the IDM, we can set  $U \simeq 0$  and we can calculate the contribution of the IDM as [4]

$$\begin{aligned} \Delta T &= \frac{1}{32\pi\alpha v^2} \left[ F(M_{H^\pm}^2, M_A^2) + F(M_{H^\pm}^2, M_X^2) - F(M_A^2, M_X^2) \right], \quad F(x, y) = \frac{x+y}{2} - \frac{xy}{x-y} \log \frac{x}{y}, \\ \Delta S &= \frac{1}{2\pi} \int_0^1 x(1-x) \log \left[ \frac{xM_X^2 + (1-x)M_A^2}{M_{H^\pm}^2} \right] dx. \end{aligned} \quad (9)$$

In the fully degenerate limit ( $M_X = M_A = M_{H^\pm}$ ),  $\Delta T = \Delta S = 0$ . In the limit  $M_X \ll M_A, M_{H^\pm}$  we have

$$\Delta T \simeq \frac{1}{24\pi^2\alpha v^2} M_A(M_{H^\pm} - M_A) \sim 0.05 \frac{M_A}{500\text{GeV}} \frac{\Delta M}{10\text{GeV}}, \quad \Delta S \simeq -\frac{5}{72\pi}. \quad (10)$$

The custodial  $SU(2)$  symmetry breaking parameter,  $T$ , restricts mass splitting such that one must have  $M_A \sim M_{H^\pm}$ . Specifically we take the limits from [92] (with  $U = 0$ )

$$S = 0.06 \pm 0.09, \quad T = 0.10 \pm 0.08, \quad \text{with a correlation of } +0.89. \quad (11)$$

**2): Direct searches at LEP.** The direct search constraints for the IDM are obtained by reinterpreting existing limits on the search for charginos and neutralinos at LEP. When the masses of the inert scalars is greater than the threshold for LEP-II production, these constraints are weaker and can be easily bypassed. They can be summarised as follows[60]

$$\begin{aligned} M_{H^\pm} &> 80 \text{ GeV (adopted from the charginos search at LEP-II),} \\ \max(M_A, M_X) &> 110 \text{ GeV (adopted from the neutralinos search at LEP-II),} \\ M_A + M_X &> M_Z \text{ from the } Z \text{ width and } M_A + M_{H^\pm} > M_W \text{ from the } W \text{ width.} \end{aligned} \quad (12)$$

**3): Direct searches at the LHC.** Because of the  $Z_2$  symmetry, the new scalars can only be produced in pairs in predominantly Drell-Yan like processes. The signatures[37, 43, 93] consist of large missing transverse energy associated with  $l$  leptons and possibly jets. For example

$$\begin{aligned} H^\pm X &\rightarrow W^\pm XX \rightarrow l^\pm + \cancel{E}_T, \quad l = 1 \\ AX &\rightarrow (Z)XX \rightarrow l^+ l^- + \cancel{E}_T, \quad l = 2 \\ H^\pm A &\rightarrow (W^\pm)(Z)XX \rightarrow l'^\pm l^+ l^- + \cancel{E}_T, \quad l = 3 \\ H^+ H^- &\rightarrow (W^+)(W^+)XX \rightarrow l^+ l'^- + \cancel{E}_T, \quad l = 2, \end{aligned} \quad (13)$$

have been studied [43]. The monojet final states ( $XXj, XAj$ ) signatures can be produced through  $\{gg, qq\} \rightarrow hg$  or  $hq$  with the decay  $h \rightarrow \chi\chi$ ,  $\chi = X, A$ , and is relevant only when  $\lambda_L$  is not too small ( $XXj$ ) or the mass splitting between  $A$  and  $X$  is small. The ATLAS and CMS collaborations have reported the signatures for dilepton plus  $E_T^{\text{miss}}$  scenario [94, 95]. As we stressed in [64], although the LHC experiments have not conducted dedicated searches within the IDM, their analyses can be reinterpreted within the IDM, see [64] for detail. Here we update our previous detailed study by taking into account the recent ATLAS analysis [96].

### 4): The LHC Higgs to diphoton, $\mu_{\gamma\gamma}$ .

The diphoton decay of the SM Higgs ( $h \rightarrow \gamma\gamma$ ), see Fig. 1 is also an important restriction. It receives a contribution from the charged scalars and therefore restricts the  $hH^+H^-$  coupling,  $\lambda_3$  and the mass,  $M_{H^\pm}$ . Similar contributions appear in  $pp \rightarrow Vh$  and can therefore be severely constrained.

The ratio of diphoton signal strength in the IDM is defined as

$$\mu_{\gamma\gamma} = \frac{\text{Br}_{IDM}(h \rightarrow \gamma\gamma)}{\text{Br}_{SM}(h \rightarrow \gamma\gamma)}. \quad (14)$$

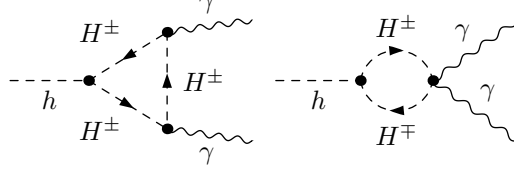


FIG. 1: The new Feynman diagrams introduced by IDM for  $h \rightarrow \gamma\gamma$  process at the one loop level.

The theoretical expression for  $\text{Br}_{\text{IDM}}(h \rightarrow \gamma\gamma)$  can be found in Refs. [23, 97] and the branching fraction in the SM is taken  $\text{Br}_{\text{SM}}(h \rightarrow \gamma\gamma) = (2.27 \pm 0.05) \times 10^{-3}$ . The Higgs diphoton signal strength from ATLAS and CMS has been reported  $\mu_{\gamma\gamma}^{\text{ATLAS}} = 0.99^{+0.15}_{-0.14}$  [98] and  $\mu_{\gamma\gamma}^{\text{CMS}} = 1.18^{+0.17}_{-0.14}$  [99]. We impose the combined limit

$$\mu_{\gamma\gamma} = 1.04 \pm 0.1. \quad (15)$$

**5): Invisible Higgs decay.** This is of relevance only for  $M_X < M_h/2 \sim 62.5$  GeV. The invisible branching fraction for  $h \rightarrow XX$  process at the tree-level is expressed as

$$\begin{aligned} \text{Br}(h \rightarrow XX) &= \frac{1}{\Gamma_h^{\text{SM}}} \frac{\lambda_L^2 v^2}{32\pi M_h} \sqrt{1 - \frac{4M_X^2}{M_h^2}} \\ &= \left[ 1.183(\lambda_L \times 10^3)^2 \sqrt{1 - 0.64(M_X/50)^2} \right] \times 10^{-3} \\ &= 2.83 \times 10^{-3} \quad \text{for } M_X = 57 \text{ GeV}, \quad \lambda_L = 2.4 \times 10^{-3} \end{aligned} \quad (16)$$

where the total width of SM Higgs is taken  $\Gamma_h^{\text{SM}} = 4.07 \pm 0.16$  MeV. The decay branching ratio in Eq. 16 is limited by the experiments results from the LHC [100, 101]. We take the limit set by ATLAS[100]

$$\text{Br}_{\text{inv.}}^h < 0.107 \quad (17)$$

**6): Models A with no DM constraints. Benchmark points** While we will be studying deviations from the SM in the  $Vh$  cross sections, across a large allowed parameter space taking all the constraints we have just listed (not assuming that that  $X$  is a DM candidate) we will take three representative benchmark points (BP's) to analyse kinematical distributions. These 3 benchmark points are listed in Table I. BP1 features a fully degenerate spectrum, all the extra scalars are relatively heavy but share the same mass,  $\lambda_L$  is also relatively large. The masses in BP2 are not as heavy,  $A$  and  $H^+$  are mass degenerate and there is a 100 GeV mass splitting between  $X$  and  $A/H^+$ . BP0 has  $M_X$  light and the other two scalars degenerate and quite heavy, however  $\lambda_L$  is smaller than in the other two benchmark points.

	$M_X(\text{GeV})$	$M_A(\text{GeV})$	$M_{H^\pm}(\text{GeV})$	$\lambda_L$	$(\lambda_3, \lambda_A)$
BP0	70	571	571	1.0	(11.61, 11.61)
BP1	500	500	500	7.08	(7.08, 7.08)
BP2	220	320	320	2.31	(4.09, 4.09)

TABLE I: In case the IDM is not a model for DM, three benchmark points selected to display differential distributions for  $Vh$  production at the LHC. The value of  $\lambda_2$  has no impact for the electroweak NLO calculation.

## 7): Dark Matter constraints

**a): Dark matter Relic Density** The lightest neutral scalar  $X$  could be a good DM candidate. To qualify it must meet the relic density,  $\Omega h^2$ , requirement which we calculate within the freeze-out scenario. We calculate such contributions with micrOMEGAs[102–106]. micrOMEGAs takes the annihilation cross sections at tree-level, albeit with an effective (electromagnetic) coupling at  $\alpha(M_Z) \sim 1/128.07$  instead of the on shell coupling in the Thomson limit  $\alpha \sim 1/137.036$ . However we have demonstrated in Ref. [64] that radiative corrections are not negligible. We

therefore include a theoretical uncertainty of 20% to be added to the experimental uncertainty on the relic density determination and require

$$0.096 < \Omega h^2 < 0.144. \quad (18)$$

**b): Dark matter direct detection.** The spin-independent DM nucleon cross section proceeds through the SM Higgs. It can be written as

$$\sigma_{SI}^h \sim \left( \frac{\lambda_L 10^3}{M_X/100\text{GeV}} \right)^2 \times 8.53 \times 10^{-49} \text{ cm}^2. \quad (19)$$

This gives a strong constraint on  $\lambda_L/M_X$ . We have updated this constraint using the latest data given by the LZ experiment in 2022 [107]. The constraint can be approximately cast as

$$\sigma_{SI}^{\text{LZ}} < 3 \times 10^{-47} \cdot (M_X/100\text{GeV}) \text{ cm}^2. \quad (20)$$

for a DM mass in the region  $40 < M_X < 100 \text{ GeV}$ , improving slightly until the minimum at 30 GeV. We have imposed the constraint

$$|\lambda_L| \times 10^3 < 6 \times (M_X/100 \text{ GeV})^{3/2} \rightarrow |\lambda_L| < |\lambda_L^{\text{max}}| = 0.0035, \text{ for } M_X = 70 \text{ GeV}. \quad (21)$$

The direct detection cross section needs to be rescaled when the relic density of DM is not completely supplied by IDM, when we assume that the latter accounts for no less than 50%, this constraint has

$$\lambda_L < \lambda_L^{\text{max}} \sqrt{\frac{\Omega_{DM}^{\text{Planck}}}{\Omega_X}}, \quad (22)$$

where the  $\Omega_X$  and  $\Omega_{DM}^{\text{Planck}}$  denote the relic density of IDM and that come from the Planck data, respectively. Because the former is greater than the latter, it is clear that the restriction from Eq. 22 is weaker than Eq. 16.

In the case where  $M_X \sim M_A \sim M_{H^\pm} \gg M_W$  there are large one-loop electroweak corrections to the scattering cross section [24, 108] that can be dominant<sup>1</sup>. The latter cross section only depends on the gauge coupling and the Higgs mass. In these limiting cases the cross section is driven by the gauge interaction and only depends on the SM parameters. With  $M_h = 125 \text{ GeV}$  the one-loop result gives [55, 108]

$$\sigma_{Xn}^g = 8.88 \times 10^{-47} \text{ cm}^2. \quad (23)$$

We take this to be a valid approximation for  $M_X > 300 \text{ GeV}$ . In this range of masses this contribution passes the LZ2022 limit. For the tree-level contribution to be larger one needs

$$\lambda_L \times 10^2 > M_X(\text{GeV})/100 \quad (24)$$

We thoroughly studied the allowed parameter space when DM constraints are imposed beyond tree-level considerations. After the constraints are updated there are still two windows. A low mass,  $M_X < M_W$ , DM candidate [65] and high mass  $M_X > 500 \text{ GeV}$  [47]. There is no intermediate mass range  $M_W < M_X < 500 \text{ GeV}$  DM candidate in the IDM. The key characteristic for all possible DM candidates in both allowed mass ranges is that  $\lambda_L$  is at least two orders of magnitude smaller than what we considered for the IDM without the DM constraints.

### 8): Models B with added DM constraints. Benchmark points

	$M_X(\text{GeV})$	$M_A(\text{GeV})$	$M_{H^\pm}(\text{GeV})$	$\lambda_L(10^{-3})$	$(\lambda_3, \lambda_A)$
BP3	59	113	123	1.0	(0.38, 0.31)
BP4	60	68	150	0.0	(0.62, 0.03)
BP5	550	551	552	19.3	(0.09, 0.06)

TABLE II: Three benchmark points that satisfy all constraints including the DM constraint.

<sup>1</sup> In [32] beyond tree-level calculations were performed on the rather constrained case with  $M_h \simeq 2M_X$ .

While we will scan over a large parameter space including the DM constraints for the indirect effects in  $Vh$  production at the LHC, we will illustrate the results for three benchmark points taken from our studies in [65] and [47], see Table II.

### III. HIGGS-STRAHLUNG IN THE SM: QCD AND EW 1-LOOP CORRECTIONS

#### A. A recap of precision calculations in the SM for $Vh$ processes at the LHC

Precision calculations of Higgs-strahlung processes in the SM span a period of almost four decades. These calculations cover both QCD calculations [109–141] and electroweak corrections [142–147]. The improvements in the calculations within the SM extended the results of inclusive cross sections to exclusive distributions including  $W/Z$  and Higgs decays. The state-of-the art is the relatively recent computation of the  $N^3\text{LO}$  [139] and the higher order correction to the  $gg$  induced  $ZH$  channel [140, 141, 148–152]. While the latter is a one-loop process at leading order it nonetheless represents about 6% of the yield due to the importance of the  $gg$  luminosity at the LHC. At LO it suffers from a large scale uncertainty, hence the need for the new calculations. As is known the largest corrections for  $Vh$  are the NLO QCD corrections which are the same as those in Drell-Yan NLO production, higher order (QCD) corrections are comparatively quite modest but reduce quite considerably the scale variation. In contrast the NLO EW corrections are in the order of a few per-cent but nonetheless quite important making these processes ideal places to study variations due to New Physics.

#### B. Our general approach to NLO QCD and electroweak corrections

While our motivation is to weigh how much the contributions from the IDM in  $Vh$  production at LHC can be, it is important to show that our code can perform automatic calculations both in the SM and the IDM (as prototype of a New Physics model). The implementation of the different contributions of the radiative corrections in the code borrows from textbook techniques that are put together to serve as checks of the result at different steps of the automation. Such a combined study allows to bring forth how different contributions in the SM ( $gg, \gamma q$  induced,...) are impacted as well as to give a measure of the scale and pdf uncertainties. In that respect one can also attempt to match the renormalization scale such that one recovers the  $N^3\text{LO}$  calculation for, at least the inclusive,  $Vh$  cross sections.

Our computation of the different contributions to  $Vh$  production at the LHC is based on the automatic tool SloopS [55, 77–84]. SloopS relies on LanHEP [153–158] for the model definition. It relies on the bundle of packages based on FeynArts [159], FormCalc [160] and LoopTools [161] for the one-loop calculations. LanHEP implements the complete set of all (ultraviolet) counterterms of the model so that full one-loop renormalisation is implemented. For the electroweak sector this can be the on-shell (OS) or a mixed  $\overline{MS}$  - OS scheme. We will come back to these issues. Our implementation of the IDM model (including its renormalisation)<sup>2</sup> has been detailed in [64]. For QCD, with the processes at hand, a full *standard*  $\overline{MS}$  scheme is taken with a renormalisation scale  $\mu_R$  and a strong coupling constant defined as  $\alpha_s(\mu_R^2)$ . The latter is calculated according to [162] with  $n_f = 5$  active flavours and 4-loop beta function [163]<sup>3</sup>.

Until now SloopS has been exploited for EW corrections to the SM and a host of renormalisable BSM extensions and also QCD corrections for DM calculations. The latter were essentially QED type corrections for which the infrared singularities are captured with a vanishingly small photon mass and collinear singularities further regulated with fermion masses. We have now extended SloopS such that applications to hadronic collisions is possible. In particular one can now exploit SloopS to handle massless partons. First, for the renormalisation of the electroweak sector we use  $G_\mu$  as input parameter *in lieu* of the electromagnetic fine structure defined in the Thomson limit. The other important extension is the use of dimensional regularisation to handle infra-red and collinear singularities for the virtual (in our case a  $2 \rightarrow 2$  process) and the radiation part (in our case a  $2 \rightarrow 3$  process).  $d = 4 - 2\epsilon_{\text{IR}}$  is applied to both the QCD and the electroweak (QED) corrections. To have extra (redundant) checks on the calculations

<sup>2</sup> Users can also access the working files and examples as explained on the wikipedia below  
[https://lapth.cnrs.fr/projects/PrecisionCalculations/idm\\_at\\_1loop](https://lapth.cnrs.fr/projects/PrecisionCalculations/idm_at_1loop)

<sup>3</sup> A 2-loop  $\beta$  function would have been sufficient in accordance with the NLO PDF evolution.

we implement two techniques for the radiation part:

- A two-cutoff phase space *slicing* method (TCPSS), with parameters  $(\delta_s, \delta_c)$  [88], where phase space is decomposed into a soft infrared region  $S$  where the energy of the extra parton, a gluon  $g$  here, is required to satisfy  $E_g < \delta_s \sqrt{\hat{s}}/2$ .  $\hat{s}$  is the partonic Mandelstam  $s$ .  $\delta_s \ll 1$  is chosen as small as possible in order for the analytical general approximation to be valid. The hard region ( $H$ ),  $E_g > \delta_s \sqrt{\hat{s}}/2$ , generally contains collinear singularities. If so, like the case at hand, this region is further subdivided into a (hard) collinear region ( $HC$ ) and a hard non-collinear region ( $H\bar{C}$ ). This subdivision is set by a cut  $\delta_c$  on the virtuality of a pair of partons. For our processes for instance, with  $i, j$  being the initial partons, the requirement is  $(\hat{s}_{ig}, \hat{s}_{jg}) \leq \delta_c \hat{s}, \hat{s}_{ij} = (p_i + p_j)^2$ . Our default implementation is  $\delta_c = \delta_s/50$ .  $S$  and  $HC$  combine with the virtual corrections and serve to (re)define the PDF's, introducing a factorisation scale,  $\mu_F$ . The initial state collinear singularities are absorbed into the bare parton distribution functions(PDFs) leaving a finite remainder which is written in terms of modified parton distribution functions(PDFs).  $H\bar{C}$  is amenable to a  $2 \rightarrow 3$  Monte-Carlo integration in  $d = 4$ . For the numerical integration of the hard region to be stable  $\delta_s$  can not be taken infinitesimally small. Therefore we usually take different values of small enough  $\delta_s$  until the result of adding the soft contribution and the hard contribution does no longer depend on the *small* value of  $\delta_s$  and a plateau in  $\delta_s$  is reached for the combined contributions. We will show explicitly how precisely a  $\delta_s$  independent result is obtained both for the QCD and QED corrections.

To sum up, NLO (say QCD) cross section in the TCPSS approach is obtained as

$$\begin{aligned} \sigma^{\text{NLO}} &= \sigma^{\text{LO}} + \Delta\sigma^{\text{NLO}} \\ \Delta\sigma^{\text{NLO}} &= \Delta\sigma_{\text{TCPSS}}^{\text{NLO}} = \sigma_V\left(\frac{1}{\epsilon_{\text{IR}}}, \frac{1}{\epsilon_{\text{IR}}^2}\right) + \sigma_S\left(\delta_s, \frac{1}{\epsilon_{\text{IR}}}, \frac{1}{\epsilon_{\text{IR}}^2}\right) + \sigma_{\text{HC}}(\delta_s, \delta_c, \frac{1}{\epsilon_{\text{IR}}}) + \sigma_{H\bar{C}}(\delta_s, \delta_c). \end{aligned} \quad (25)$$

$(d\sigma^{\text{LO}}) \sigma^{\text{LO}}$  is the leading order (differential) cross section. The virtual correction  $\sigma_V$  includes UV renormalisation.

In the case of the electroweak corrections, there is an added IR divergence in the case of  $W^\pm$  in the final state.  $\sigma_S$  in Eq. 25 needs then to be modified to take into account the added final state radiation such as

$$d\sigma_S = F_S(\epsilon_{\text{IR}}) \sum_{f, f' = q_i, q_j, W^\pm} d\sigma^{\text{LO}} \int \frac{-p_f \cdot p_{f'}}{p_f \cdot p_\gamma p_\gamma \cdot p_{f'}} dPS. \quad (26)$$

$PS$  is the element of phase space in  $d$ -dimension integrated over the (soft) photon energy  $E_\gamma < \delta_s \sqrt{\hat{s}}/2$ .  $F_S$  is a universal factor.

To this first type of corrections to the  $q\bar{q}$  initiated production, a complete order ( $\mathcal{O}(\alpha, \alpha_s)$ ) involves  $qg, q\gamma$  induced production. Although infra-red finite, these contain a collinear singularity which is treated in a similar manner to the  $q\bar{q}$  case: dimensional regularisation for the  $HC$  and redefinition of the PDFs with the corresponding splitting functions, the  $H\bar{C}$  are calculated numerically in 4-dimensions. We will also check the  $\delta_c$  independence of the total result of this contribution which writes as Eq. 25 but with  $\sigma_V = \sigma_S = 0$  (and  $\delta_s \rightarrow 0$ ) in the last two terms. The other corrections,  $gg, \gamma\gamma$  induced production, are finite in a NLO approach.

- The other approach for the infrared/collinear singularities is the more efficient dipole subtraction (DS) method. The efficiency and accuracy of the method lies in the fact that subtraction is essentially achieved before integration over phase space is performed. DS is carried through à la Catani-Seymour[85–87, 164–168]. For the EW corrections, we adapt the dipole formulae in QCD provided in Refs. [85–87] in a straightforward way (change of gauge coupling/colour factor) to the case of dimensionally regularized photon emission. The implementation of the subtraction includes a “cut” parameter<sup>4</sup>  $\alpha'$ ,  $0 < \alpha' \leq 1$ , which serves to check the  $\alpha'$  independence of the final result. As known, the basic idea is to construct a local simple counterterm  $d\sigma^A$  that captures the universal structure of the infrared/collinear singularity of the radiation. The universal structure of the radiation (from a quark or a gluon for QCD or electrically charged particles for EW) is carried by the corresponding  $dV_{\text{dipole}}$  that factors the tree-level differential cross section. We will have to sum over all possible radiations. For a  $2 \rightarrow 2$  process like the case at hand

<sup>4</sup> This corresponds to the parameter  $\alpha$  in the original proposal[165, 166], introduced to control the size of the dipole phase space.

which will involve a radiation of a  $2 \rightarrow 3$  type, in the dipole implementation Eq. 25 turns into

$$\Delta\sigma^{\text{NLO}} = \Delta\sigma_{\text{Dipole}}^{\text{NLO}} = \sigma_V + \sigma_R = \int_2 \left( d\sigma_V + \underbrace{\int_1 d\sigma^A}_{d\sigma_{\text{IntDipole}}} \right) + \int_3 \underbrace{(d\sigma_R - d\sigma^A)}_{d\sigma_{\text{Dipole}}}, \quad \text{and} \quad d\sigma^A = \sum_{\text{dipoles}} d\sigma^{\text{LO}} \otimes dV_{\text{dipole}}. \quad (27)$$

The subscripts for the integrals refer to the dimensionality of phase-space.  $\otimes$  represents phase space convolutions and sums over color and spin indices. With the  $\alpha'$  implementation the subtraction term is not unique ( $\alpha'$  dependent) but as long as it captures the singularities it does the job.  $\alpha'$  can be defined through some kinematic variable entering the dipole. For example, for the process  $u(p_1) + \bar{u}(p_2) \rightarrow g(p_g)Zh$ , the kinematic factor for dipole  $i$  can be taken as  $K_i = 2p_i \cdot p_g / \hat{s}$  ( $i = 1, 2$ ), such that  $d\sigma_i^A = d\sigma^{\text{LO}} \otimes dV_{\text{dipole}}^i (K_i < \alpha')$  ( $d\sigma_i^A = 0$  for  $K_i > \alpha'$ ). Similarly to the case for TCPSS (see Eq. 25), we can write

$$\Delta\sigma_{\text{Dipole}}^{\text{NLO}} = \left( \sigma_V \left( \frac{1}{\epsilon_{\text{IR}}}, \frac{1}{\epsilon_{\text{IR}}^2} \right) + \sigma_{\text{IntDipole}}(\alpha', \frac{1}{\epsilon_{\text{IR}}}, \frac{1}{\epsilon_{\text{IR}}^2}) \right) + \sigma_{\text{Dipole}}(\alpha'). \quad (28)$$

For all three  $pp \rightarrow W^\pm h, Zh$  processes, the NLO QCD correction to the  $q\bar{q}^{(\prime)}$  only involve Initial(emitter)-Initial(spectator) type contributions. When generalising to the EW (QED) corrections, in the  $W^\pm h$  case, extra combinations of dipole are needed due to the infrared singularity from photon radiation off the charged (massive)  $W^\pm$ . As we will demonstrate the handling of the infra-red/collinear singularities for  $pp \rightarrow Vh$  performs extremely well. Not only  $\alpha'$  independence serves as an internal test of DS, as is the *plateau-ing* in  $\delta_s$  and  $\delta_c$  for TCPSS, but the agreement between the two methods is an extra independent test. We have tested this approach on a selection of  $2 \rightarrow 2$  processes. Work is in progress to make this approach fully automatic in SloopS for a general process beyond  $2 \rightarrow 2$  processes, especially for the fast and very efficient  $\alpha'$ -DS implementation.

### C. Standard Model Parameters

This is a good place to define and set the SM parameters relevant for the processes we will study and to obtain the numerical values we have found.

The standard model input parameters will be taken as [169]

$$\begin{aligned} M_Z &= 91.1876 \text{ GeV}, & M_W &= 80.385 \text{ GeV}, & M_h &= 125 \text{ GeV} \\ M_t &= 173.21 \text{ GeV}, & G_\mu &= 1.1663787 \times 10^{-5} \text{ GeV}^{-2}. \end{aligned} \quad (29)$$

All fermions, but the top, are taken massless. The Cabibbo-Kobayashi-Maskawa (CKM) matrix is taken to be the unit matrix. We will use different PDFs sets with  $\alpha_s(M_Z) = 0.118$  via LHAPDF6 [163] in the  $n_f = 5$  fixed-flavour scheme in both the LO and NLO predictions. We will take the renormalisation,  $\mu_R$ , and factorisation,  $\mu_F$ , scales equal and track, as is done in Reference [139] the scale dependence through the parameter  $x_{R/F}$  defined as

$$\mu_R = \mu_F = x_{R/F} (M_V + M_h). \quad (30)$$

We will vary  $x_{R/F}$  in the range  $1/8 \leq x_{R/F} \leq 5$ . Unless otherwise stated, the cross sections refer to the use of NNPDF31-1uxQED PDFs set [170, 171]. We will then take  $x_{R/F} = 2$  for reasons we will explicit in due course. All our figures are for a run made for the LHC at  $\sqrt{s} = 13$  TeV.

### D. Leading Order, LO

In the five (massless) flavour scheme, associated Higgs-vector boson production, Higgs-strahlung, at LO (partonic) is of a Drell-Yan type

$$q_i \bar{q}_j \rightarrow Vh, \quad V = Z, W^\pm,$$

where the  $q_i, q_j = u, d, s, c, b$ . It is shown in Fig. 2.

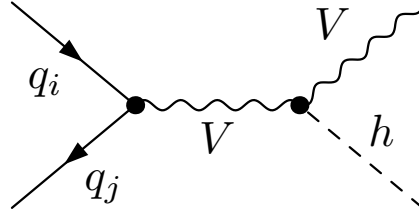


FIG. 2: Tree level Feynman diagrams for Higgs-strahlung process in the five flavour scheme. The  $q_{i(j)}$  represents all (non top) quark flavours and anti-quarks and  $V = Z, W^\pm$ .

Observe, again, that at this first order, the cross section is exactly the same in the IDM as in the SM. This means also that the renormalisation of the (extra) parameters of the IDM (masses of the scalars and the couplings  $\lambda_L$  and  $\lambda_2$ ) are not needed for these processes. All effects of the IDM will be indirect and will only affect the electroweak corrections. Because no extra coloured degree of freedom is brought by the IDM, the NLO QCD corrections in the IDM and the SM are the same. Nonetheless, we will carry through the different steps of the NLO calculations. This will also serve to highlight how our general approach to loop calculations with the help of SloopS which we have developed in the previous section, in particular of the soft/collinear singularities, comes into play.

### E. NLO QCD corrections

#### 1. Virtual QCD corrections and the corresponding bremsstrahlung real corrections

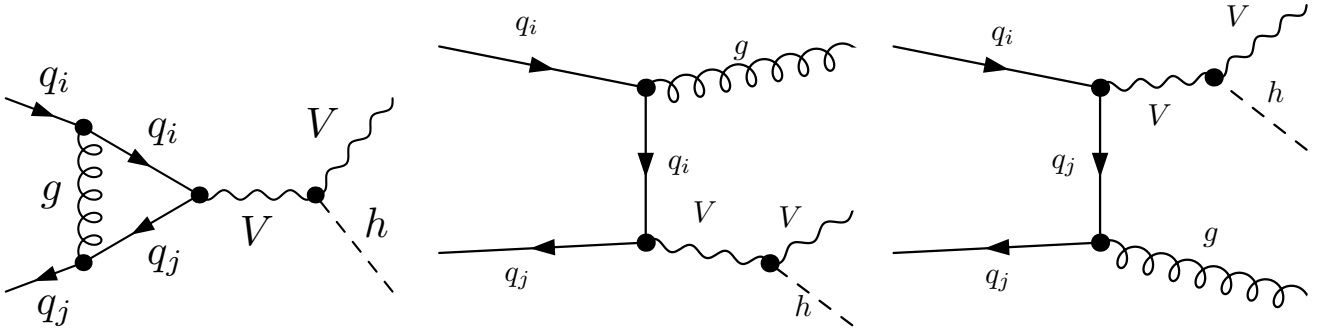


FIG. 3: Feynman diagrams for the virtual QCD correction (left) and real bremsstrahlung (right) for Higgs-strahlung.  $V = W^\pm, Z$ .

The one-loop QCD corrections consist essentially of the vertex correction shown in Fig. 3. In SloopS the two-point self energy corrections on the external legs is combined with the counterterm and is not shown. The corresponding real corrections are shown also in Fig. 3.

The infrared/collinear terms involve the splitting function  $P_{q\bar{q}}$  to combine with the corresponding  $q\bar{q}$  luminosities. The induced  $qg$  involve the  $qg$  splitting functions  $P_{qg}$ .

In combining the virtual and real corrections we have checked the slicing method,  $\Delta\sigma_{\text{TCPSS}}^{\text{NLO}}$  Eq. 25, against the dipole subtraction  $\Delta\sigma_{\text{Dipole}}^{\text{NLO}}$  Eq. 28. The result for the  $q\bar{q}$  initiated  $W^-h$  production is shown in Fig. 4. The two methods agree extremely well, within  $1\sigma$ . We however underline the efficacy of the dipole subtraction which furnishes a stable result for all values of  $\alpha'$ . In the slicing method, convergence occurs for smallest values of  $\delta_s$ , around  $10^{-4}$  while smaller values give a larger Monte-Carlo error, see Fig. 4.

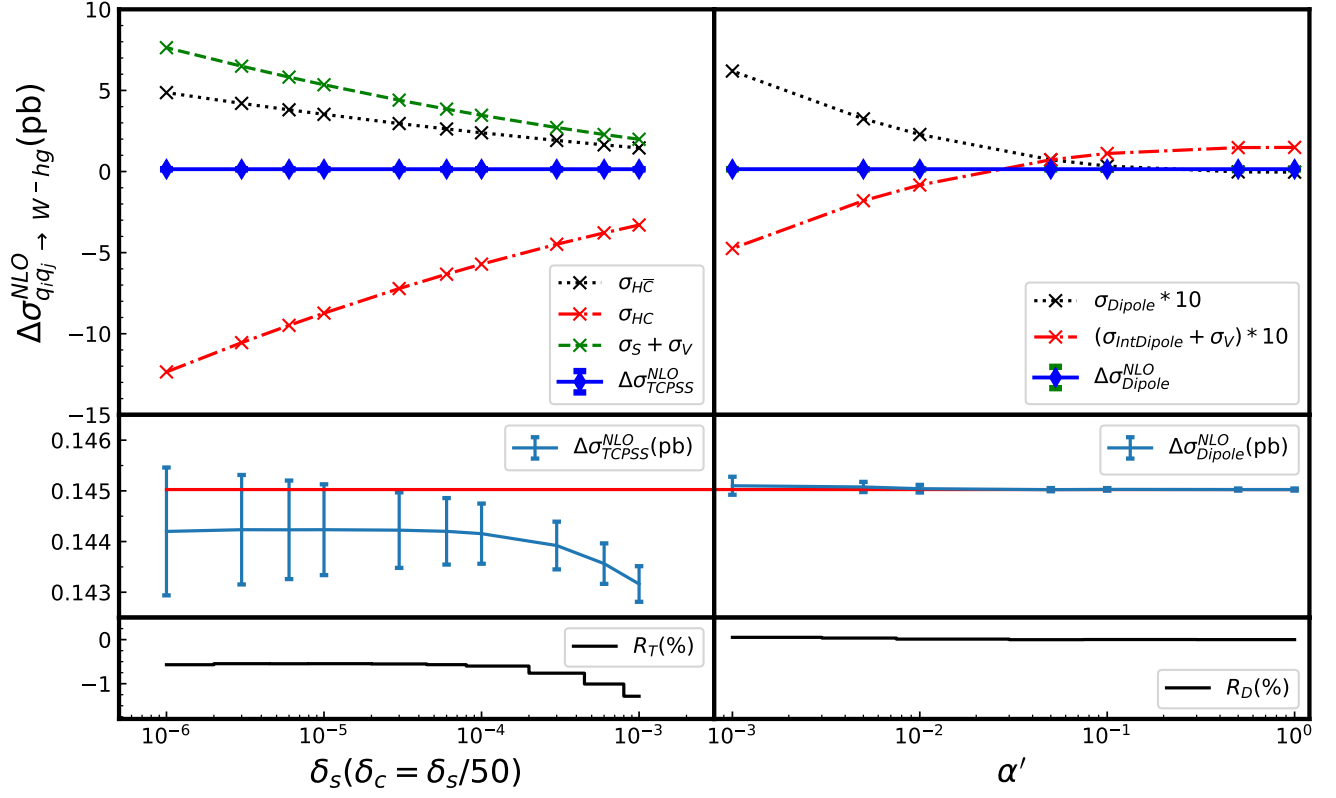


FIG. 4: Comparing the slicing method and dipole subtraction for QCD radiative corrections to  $q_i q_j \rightarrow W^- h g$ . In the upper panels, we show the results for each part for the DS and the TCPSS methods. The middle panels zoom in on the total contribution ( $\sigma_{\text{TCPSS}}^{\text{NLO}}$  and  $\sigma_{\text{Dipole}}^{\text{NLO}}$ ) of each method together with its Monte-Carlo uncertainty. Taking  $\sigma_{\text{Dipole}}^{\text{NLO}}(\alpha' = 1)$  as a reference. The lower panels show, in %, the deviations from this reference point as  $R_T = \frac{\Delta\sigma_{\text{TCPSS}}^{\text{NLO}} - \Delta\sigma_{\text{Dipole}}^{\text{NLO}}(\alpha' = 1)}{\Delta\sigma_{\text{Dipole}}^{\text{NLO}}(\alpha' = 1)}$  and  $R_D = \frac{\Delta\sigma_{\text{Dipole}}^{\text{NLO}} - \Delta\sigma_{\text{Dipole}}^{\text{NLO}}(\alpha' = 1)}{\Delta\sigma_{\text{Dipole}}^{\text{NLO}}(\alpha' = 1)}$ .  $\sqrt{s} = 13$  TeV.

## 2. Real corrections: $gq$ induced contributions

The induced  $gq$  processes are shown in Fig. 5.

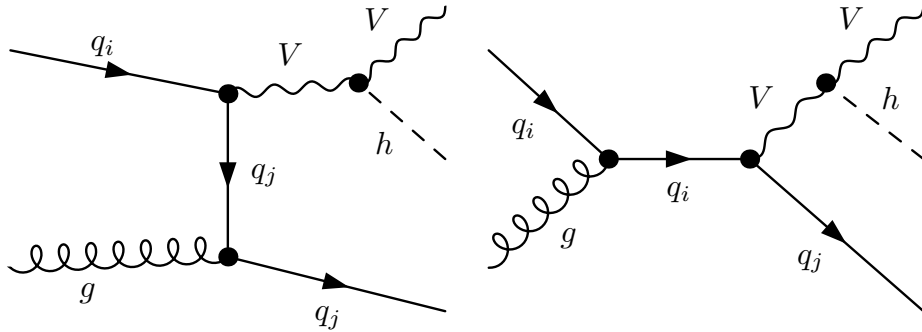


FIG. 5: Feynman diagrams of QCD (initiated) real radiation processes for Higgs-strahlung.

The collinear divergence is treated by the two methods we have just reviewed, in the absence of virtual/soft contribution terms. While the plateau in  $\delta_c$  for the TCPSS cut method is reached quickly, the dipole method is slightly more precise. The two methods agree at better than the per-mil level as Fig. 6 reveals.

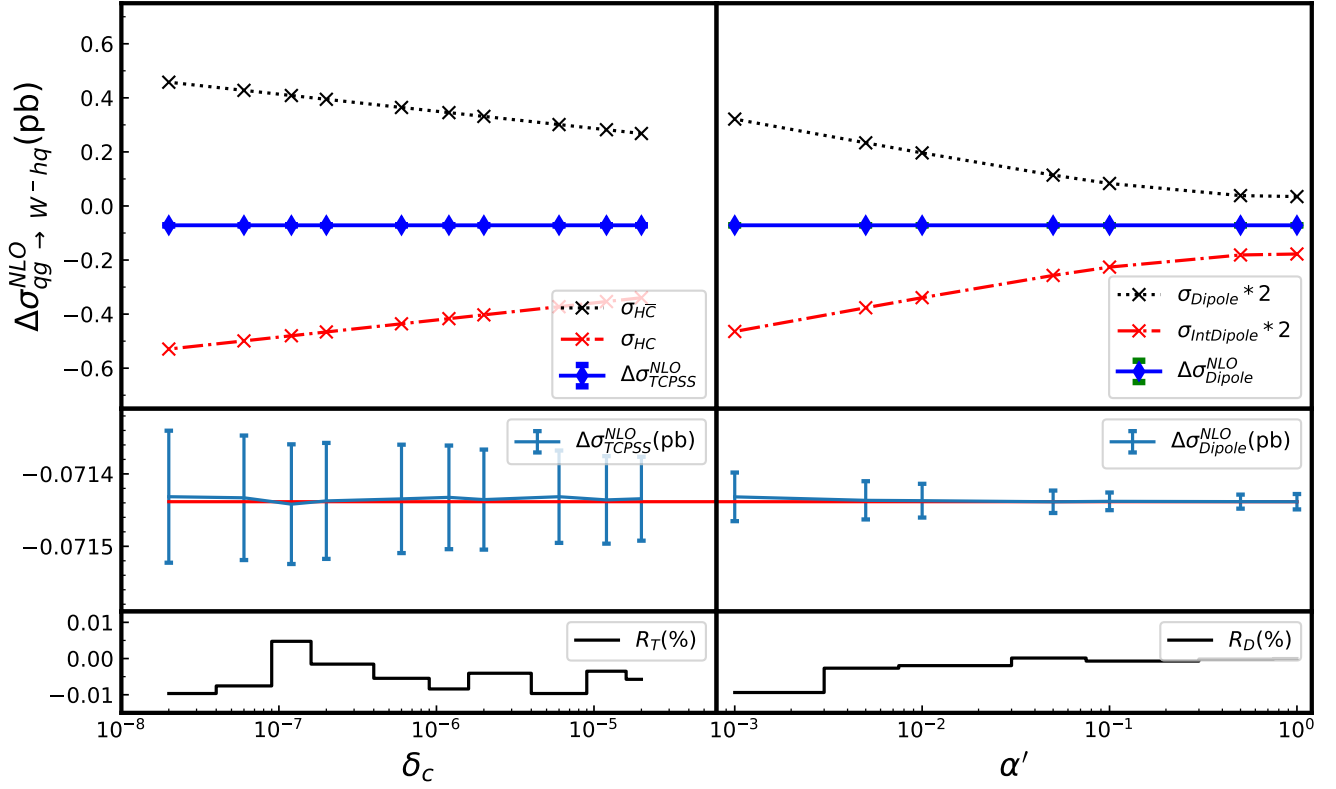


FIG. 6: As in Fig. 4. Comparing the slicing method and dipole subtraction, but for  $gq$  induced contributions.

### 3. $gg$ induced contributions: $Zh$ production

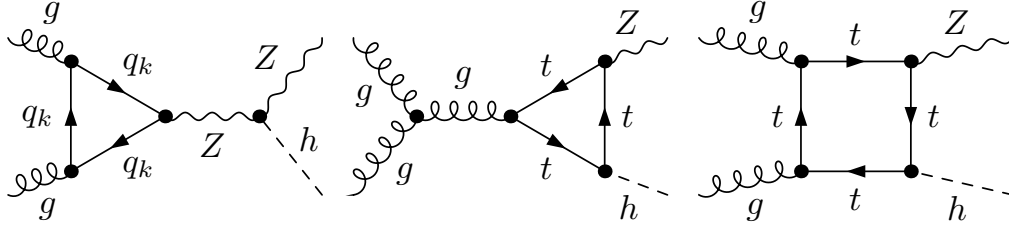


FIG. 7: The Feynman diagrams of  $gg$  induced contributions for  $Zh$  production. In the first diagram the contribution from the quarks of the first two generations (all massless) cancel. Only the top and bottom loop contribute, the vector part of  $Zgg$  (real gluons) is zero as a consequence of Landau theorem.

$Zh$  production has an additional  $gg \rightarrow Zh$  one-loop (UV and IR finite) contribution, shown in Fig. 7. The top plays an important part in this  $gg$  fusion.

### 4. Comparison with Madgraph for the NLO QCD corrections in the SM.

Taking all the QCD NLO contributions discussed in the previous section we have conducted a tuned comparison (convoluting with the same PDFs set and taking the SM parameters defined in Eq. 29) of the NLO QCD corrections between our code and Madgraph [76] on all three  $Vh$  subprocesses. The numbers we show in Table. III refer to our implementation of the dipole subtraction (as discussed above the 2-cut method gives exactly the same results). As can be seen in Table. III the agreement is excellent. The agreement is for the most part below the level of the per-mil

and the worst, is at 0.4%.

		Madgraph	SloopS
$Zh$	LO	0.6021(5)	0.6022(1)
	NLO	0.825(2)	0.824(1)
$W^-h$	LO	0.4282(4)	0.4283(1)
	NLO(QCD)	0.528(2)	0.5279(2)
$W^+h$	LO	0.6803(6)	0.6804(2)
	NLO(QCD)	0.839(3)	0.8420(4)

TABLE III: Comparison between the results of the NLO QCD corrections in Madgraph and SloopS in the SM. Cross sections are in pb. for  $Zh$ , the  $gg$  the one-loop  $gg$  initiated process is included. Here we take the renormalisation and factorisation scales as  $\mu_R = \mu_F = M_Z$ .

### 5. Scale and PDFs uncertainty.

As mentioned earlier (see section III), computations for the processes at hand have now been performed beyond NLO and beyond inclusive cross sections. The remaining uncertainties have been estimated. For the QCD contributions these uncertainties are of order 1-2%. Estimates of the uncertainties is important as the latter set sensitivity yardsticks, independently of the experimental uncertainties, above which the effect of any New Physics can be validated. Based on the NLO corrections results of the same code that derives the contributions of the New Physics we can have another look at the uncertainties with the latest PDFs. We will base our analyses on three PDFs sets: *i*) PDF4LHC21\_40 [172] which is a combination of the CT18 PDFs, the NNPDF3.1[170] and the MHST20[173] *ii*) NNPDF31-luxqed (our default set) and *iii*) MSHT20qed\_nnlo [174]. In both NNPDF31-luxqed and MSHT20qed\_nnlo the photon content is implemented with some realisation of the LUX approach[175, 176]. The latter sets permit for the incorporation of photon initiated contributions therefore making it possible to take into account the effect of both the QCD corrections and the full NLO EW. The LUX approach has allowed a much better determination of the photon content of the proton. We use PDF4LHC21\_40 not only to weigh the importance the photon initiated contribution in our processes but also to check whether the precision of the fit including the photon PDF's does not deteriorate much the overall uncertainty of the prediction due to the PDF's.

One of the uncertainty in the calculation of the cross section is the one due to the scale variation. Recall that for the scale dependence we take  $\mu_R = \mu_F$  and that we track the dependence through the parameter  $x_{R/F}$  with  $\mu_{R/F} = x_{R/F} M_{HV} = x_{R/F} (M_V + M_h)$ . As can be seen from Fig. 8 we first of all recover the large NLO QCD corrections[112, 118] and the large scale uncertainties, in particular the large corrections for  $x_{R/F} < 1$  (these are essentially the same as for the NLO QCD corrections to Drell-Yan) in all three channels. Observe that the NLO scale dependence almost plateaus when  $x_{R/F} > 1$ . Combined with the fact that, as stated before, NNLO and N<sup>3</sup>LO add in much smaller corrections, we will take  $x_{R/F} = 2$  to recover with percent precision the higher order predictions for the inclusive cross sections. Fig. 8 also shows that the PDFs uncertainty estimated, for this section, as the difference between the three PDFs sets we have chosen is at the per-mil level, in particular around the  $x_{R/F}$  values we have advocated. In any case, for us it is yet another confirmation that our code is performing well. One should keep in mind that the estimated uncertainty could be larger if  $x_F$  and  $x_R$  were varied independently, or if one looked at a specific distribution (including  $V, h$  decays).

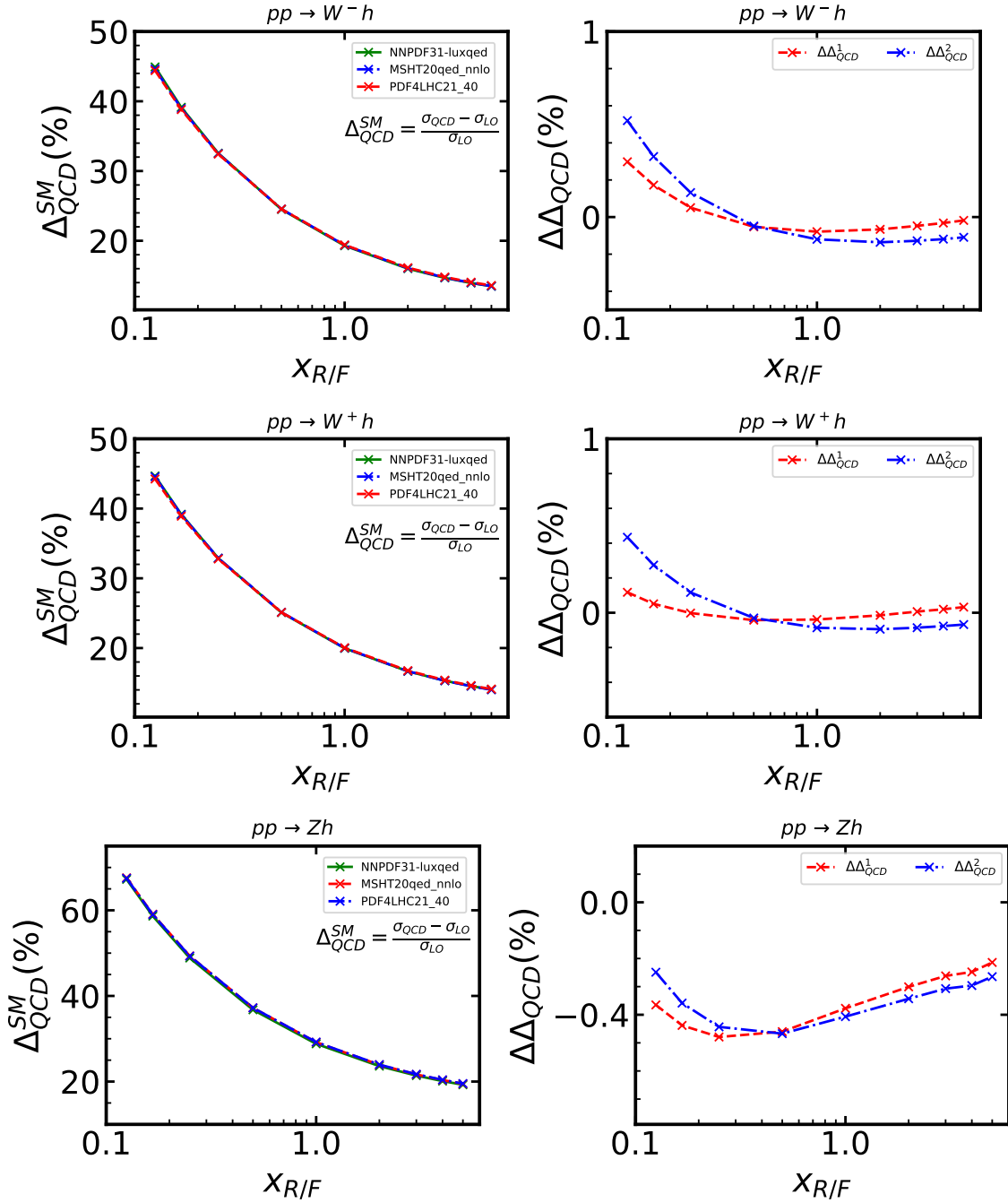


FIG. 8: The scale and PDF uncertainty of the NLO QCD (percentage) correction,  $\Delta_{QCD}^{SM}$ , for  $pp \rightarrow Vh$  process. For better visibility of the error coming from the different choices of the PDFs, we define the percentage differences (between the relative corrections) as  $\Delta\Delta_{QCD}^1 = \Delta_{QCD}^{SM}(NNPDF) - \Delta_{QCD}^{SM}(MSHT)$  and  $\Delta\Delta_{QCD}^2 = \Delta_{QCD}^{SM}(NNPDF) - \Delta_{QCD}^{SM}(PDF4LHC)$ .

## E. EW corrections in the SM

### 1. Renormalization. The $G_\mu$ scheme

The renormalisation of the IDM[64] is conducted in the On-Shell (OS) scheme with a slight variation concerning the renormalisation of the electromagnetic coupling constant  $\alpha$ . In the standard OS scheme[177] the latter is defined in the Thomson limit (vanishing photon momentum transfer). Using the Ward identity and OS condition, the

renormalization constant for the electric charge  $\delta Z_e$  is obtained as

$$\delta Z_e^{\alpha(0)} = -\frac{1}{2}\delta Z_{AA} - \frac{1}{2}\frac{s_W}{c_W}\delta Z_{ZA} = \frac{1}{2}\frac{\partial \Sigma_T^{AA}(p^2)}{\partial p^2}\Big|_{p^2 \rightarrow 0} - \frac{s_W}{c_W}\frac{\Sigma_T^{AZ}(0)}{M_Z^2}, \quad (31)$$

where the superscript relates to the  $\alpha(0)$ -scheme. For the  $A \rightarrow B$  transition  $\delta Z_{AB}$  and  $\Sigma_T^{AB}(p^2)$  are, respectively, the wave function renormalisation constants and the transverse parts of the  $A \rightarrow B$  self-energy at momentum transfer squared  $p^2$ . In applications to the LHC where we have chosen to work with massless fermions/partons, the self-energies would not be defined. A subtraction at  $p^2 = M_Z^2$  (through the running fine-structure constant  $\alpha(M_Z)$ ,  $\alpha(M_Z)$ -scheme) would be more appropriate. In fact we adopt the  $G_\mu$ -scheme with  $G_\mu$ , the Fermi constant as defined in  $\mu$  decay, as an independent parameter instead of  $\alpha(0)$ . The corresponding effective electromagnetic coupling strength is defined as [178]

$$\alpha_{G_\mu} = \frac{\sqrt{2}G_F M_W^2}{\pi} \left(1 - \frac{M_W^2}{M_Z^2}\right) = \alpha(0)(1 + \Delta r), \quad (32)$$

with the corresponding counterterm for  $\alpha$

$$\delta Z_e^{G_\mu} = \delta Z_e^{\alpha(0)} - \frac{1}{2}\Delta r. \quad (33)$$

In the usual linear gauge, with the Feynman parameter  $\xi = 1$ ,  $\Delta r$  is expressed as [178, 179]

$$\Delta r = \Pi^{AA}(0) - \frac{c_W^2}{s_W^2} \left( \frac{\Sigma_T^{ZZ}(M_Z^2)}{M_Z^2} - \frac{\Sigma_T^W(M_W^2)}{M_W^2} \right) + \frac{\Sigma_T^W(0) - \Sigma_T^W(M_W^2)}{M_W^2} + 2\frac{c_W}{s_W} \frac{\Sigma_T^{AZ}(0)}{M_Z^2} + \frac{\alpha}{4\pi s_W^2} \left( 6 + \frac{7 - 4s_W^2}{2s_W^2} \log c_W^2 \right). \quad (34)$$

In the general implementation of a New Physics model and its renormalisation, in a first stage we check that renormalisation is carried correctly in the  $\alpha(0)$  scheme by testing the UV finiteness and the gauge parameter independence of a series of processes. The latter exploits a multi-parameter gauge-fixing function in the non-linear gauge. In the context of the IDM, the reader should refer to [65]. Only then, for LHC applications, do we revert to  $\alpha_{G_\mu}$  scheme. Note also that for this class of models, the contribution to  $\mu$  decay is only to two-point functions whose contributions to  $S, T, U$  have also been independently evaluated for the parameter space of the IDM to pass the constraints, see section II B 2.

## 2. Virtual one-loop electroweak corrections

Compared to the QCD corrections, the full set of EW virtual contributions is much larger. It contains 2-point, 3-point and 4-point one-loop diagrams some of which are displayed in Fig. 9.

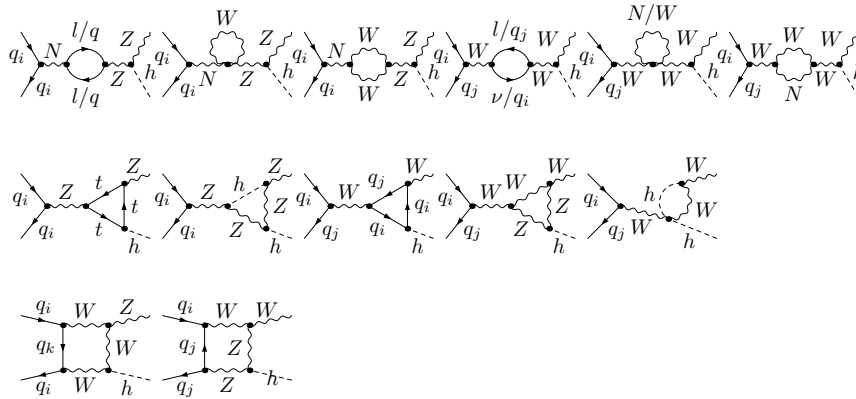


FIG. 9: Representatives of the set of EW virtual corrections for  $q\bar{q}$  annihilation for  $Wh$  and  $Zh$  production. The first row contains the self-energy diagrams, the second the triangles and the third is a collection of boxes.  $N = Z, \gamma$ .

Another set is displayed in Fig. 10. The latter (with photonic contributions) exhibits infra-red (and collinear singularities) which must combined with the real corrections.

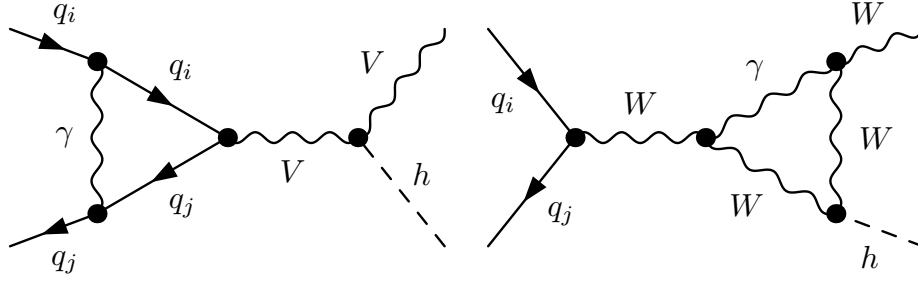


FIG. 10: Representatives of the virtual electroweak corrections with IR divergences. Note that for  $Wh$  production an additional radiation for the charged  $W$  also leads to an infrared contribution. The latter because the  $W$  is massive does not contain a collinear singular part.

### 3. Real photonic corrections for $q\bar{q}$ annihilation

The Feynman diagrams of EW real corrections for Higgs-strahlung are shown in Fig. 11. Compared with the real (initial state) QCD corrections, there are extra contributions with final state photon radiations for  $W^\pm h$  productions. For radiations of initial photon in Fig. 11, the subtraction of IR divergence are similar to the QCD case, see Sec. III E 1

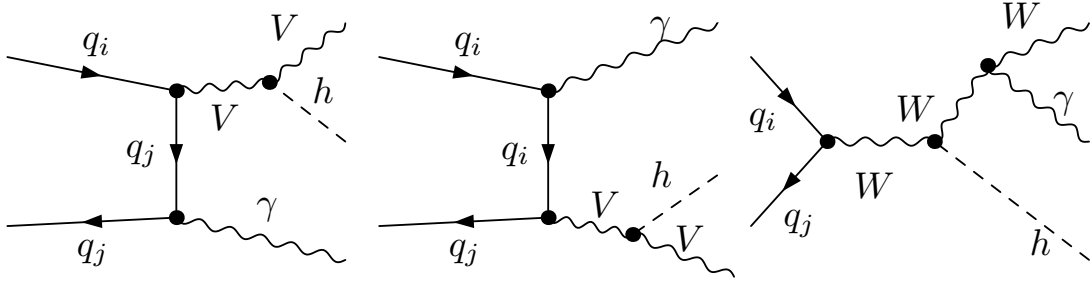


FIG. 11: Representatives of the real electroweak corrections with IR divergences. The first graph combines with the first one of Fig. 10 and the photon emitted from the  $W$  combines the second graph of Fig. 10.

for TCPSS and DS schemes. We only need to substitute the electric charge for the color factors and the strong coupling. However, the  $W^\pm h$  productions involve the contributions of final photon radiation  $W^\pm \rightarrow W^\pm + \gamma$  which include the extra soft divergence, not the collinear divergence because of the large  $W$  mass.

### 4. Combining (photonic) real and virtual corrections soft/collinear divergences

Combining the last two contributions in the electroweak case goes along the same line as what was done in the QCD, generalising and adapting to the massive  $W$  in the final state. Again we compare dipole *vs* TCPSS in the electroweak case. As expected there is good agreement, but the dipole is not only more precise but again TCPSS starts converging for extremely small values of the soft photon cut ( $\delta_s$ ), while for extremely small  $\delta_s$  the error gets larger. Nonetheless the contribution is easily computed with an error less than the per-mil, see Fig. 12

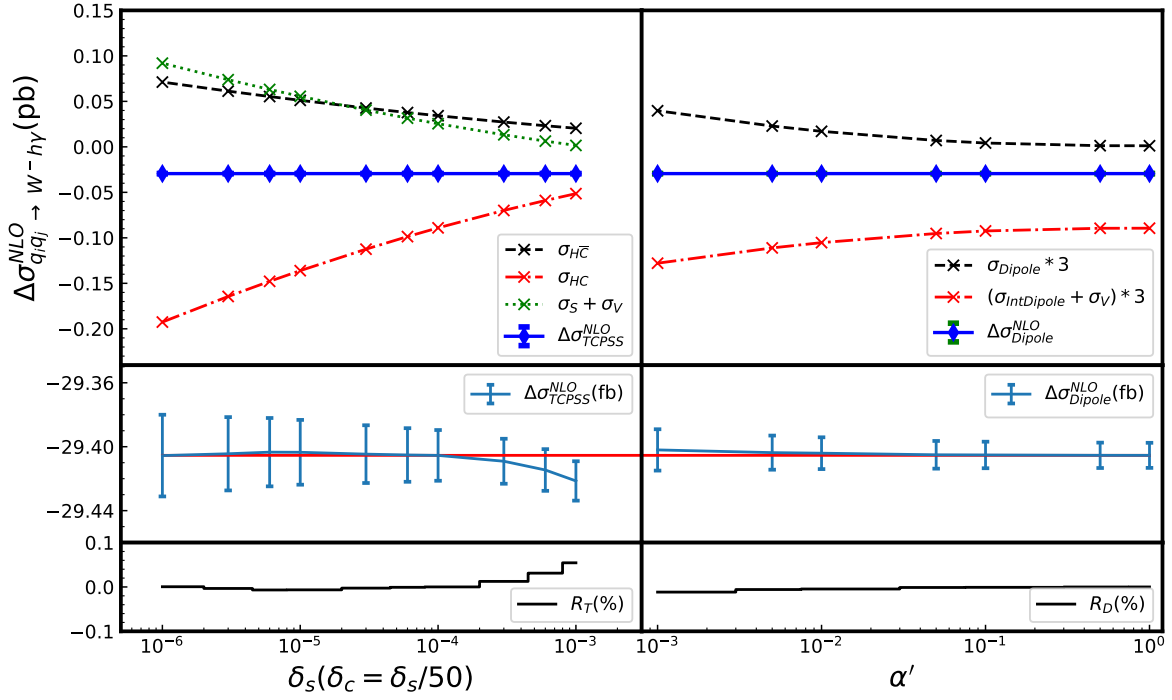


FIG. 12: As in Fig. 4 but comparing the slicing method and dipole subtraction but for the photonic corrections.  $R_{T,D}$  have the same meaning as in Fig. 4

### 5. $q\gamma$ initiated annihilation

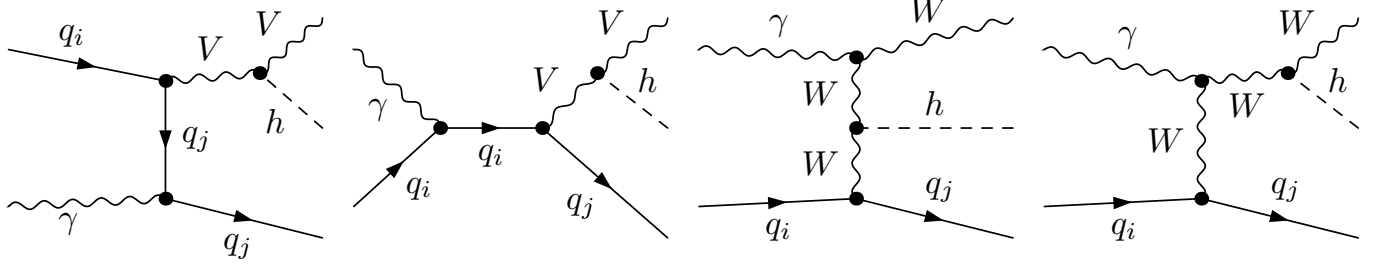


FIG. 13: Contributions to induced  $q\gamma$  annihilation. Observe the presence of  $W$  in the  $t$ -channel for the  $Wh$  production.

The application of DS and TCPSS schemes to  $q\gamma$  annihilation is totally similar to the  $qg$  case for the QCD corrections. However, a glance at the partonic contribution in the case of the photon reveals an important difference. While quark exchange, see Fig. 13 has an equivalent in the QCD case, observe the contribution of the  $t$ -channel spin-1 exchange (the  $W$ ) for  $W^\pm h$  production. For total cross sections,  $t$ -channel spin-1 exchange leads to large and constant ( $\hat{s}$  independent) cross sections. Expect therefore that a large contribution will show up in  $Wh$  channel compared to  $Zh$ , for which such spin-1 exchange is absent. Note also that the large partonic cross section in the  $Wh$  channel is due to the forward scattering region and that a  $p_T$  cut will reduce this contribution. At this point, let us just note that the application of DS and TCPSS shows, see Fig. 14, the excellent agreement between the two approaches. They both show excellent stability over 3 orders of magnitude in the respective cut-offs.

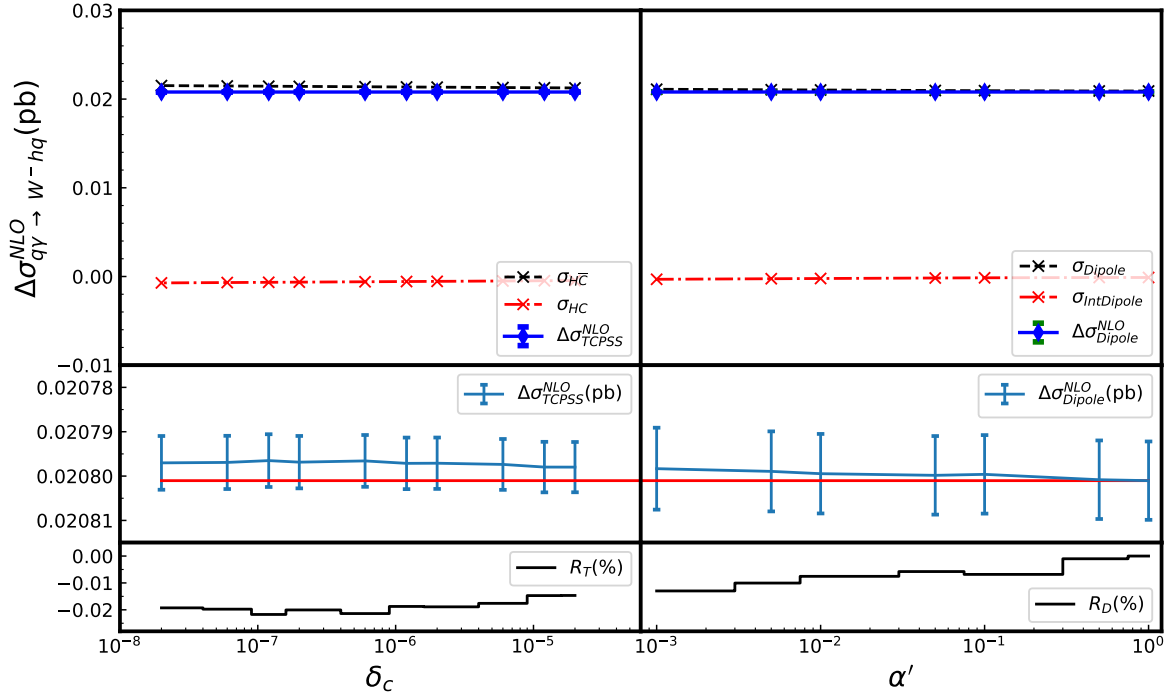


FIG. 14: Comparing the slicing method and dipole subtraction, but for induced  $q\gamma$  annihilation contributions.

#### 6. $\gamma\gamma$ induced $Zh$ production in the SM

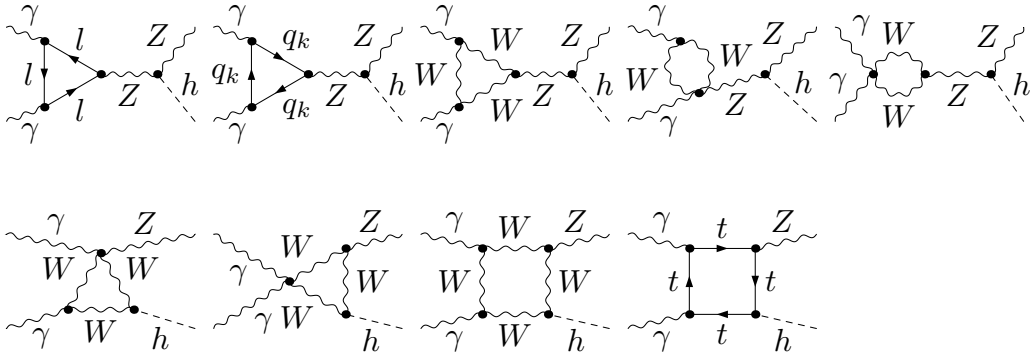


FIG. 15: Induced  $\gamma\gamma$  contributions in the case of  $Zh$  production.

For  $Zh$  production, there also are contributions from the  $\gamma\gamma$  induced as shown in Fig. 15. These contributions are totally negligible not only because these are generated at one-loop but also because the  $\gamma\gamma$  luminosity (convolution) is extremely tiny. At the end this cross section amounts to less than  $3 \times 10^{-6}$  the total  $Zh$  production at the LHC. We will not mention it in the rest of this paper.

#### 7. Results, Scale dependence and PDFs uncertainty of the electroweak corrections in the SM. Impact on the full NLO corrections

Taking all the contributions we outlined for the electroweak corrections our numerical results concerning the relative corrections for the inclusive  $Vh$  cross sections at the 13 TeV LHC are shown in Fig. 16 for our three sets of PDFs.

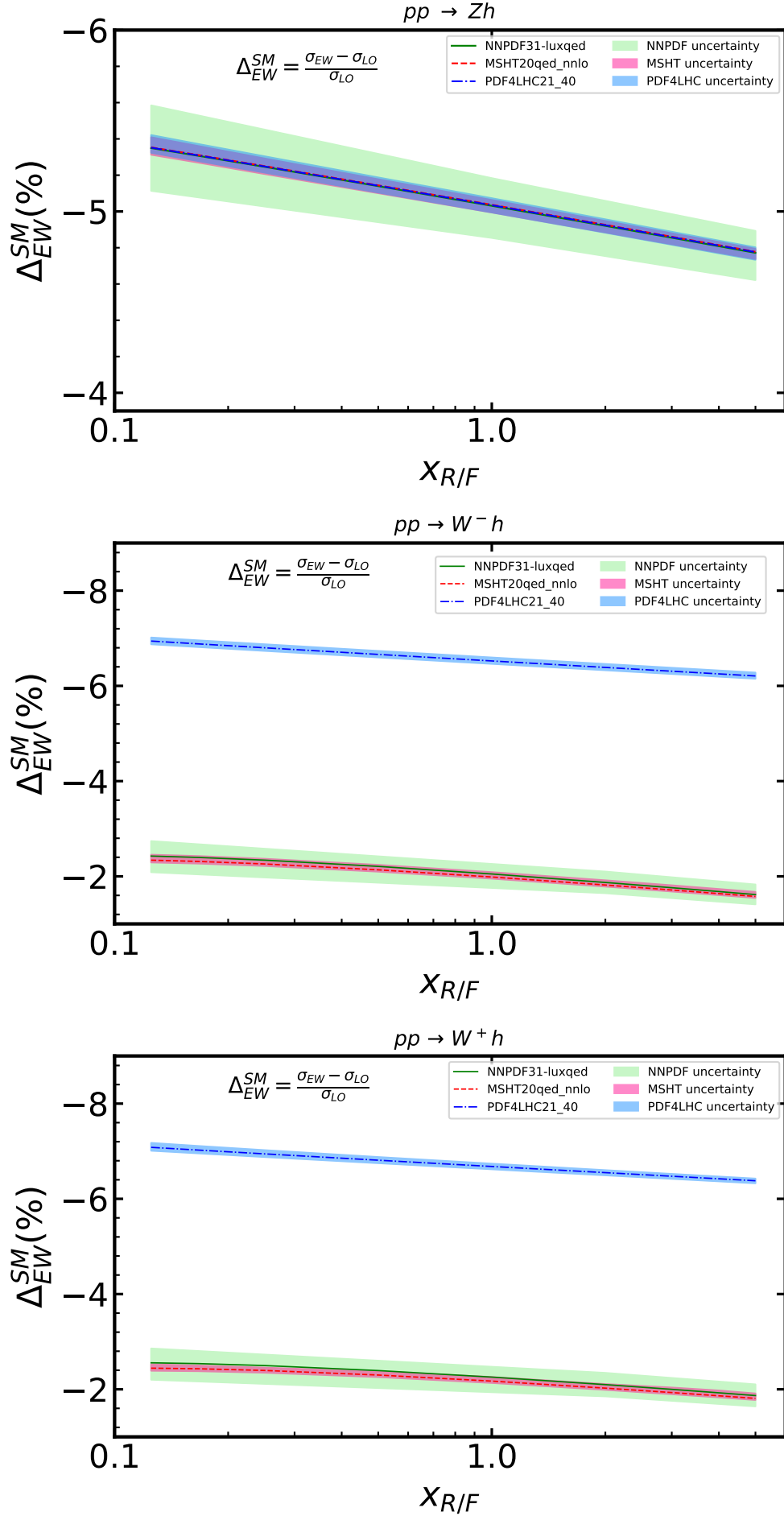


FIG. 16: The relative electroweak correction for the three  $Vh$  channels, as a function of the scale variation parameterised through

## G. Electroweak and QCD NLO corrections in the SM

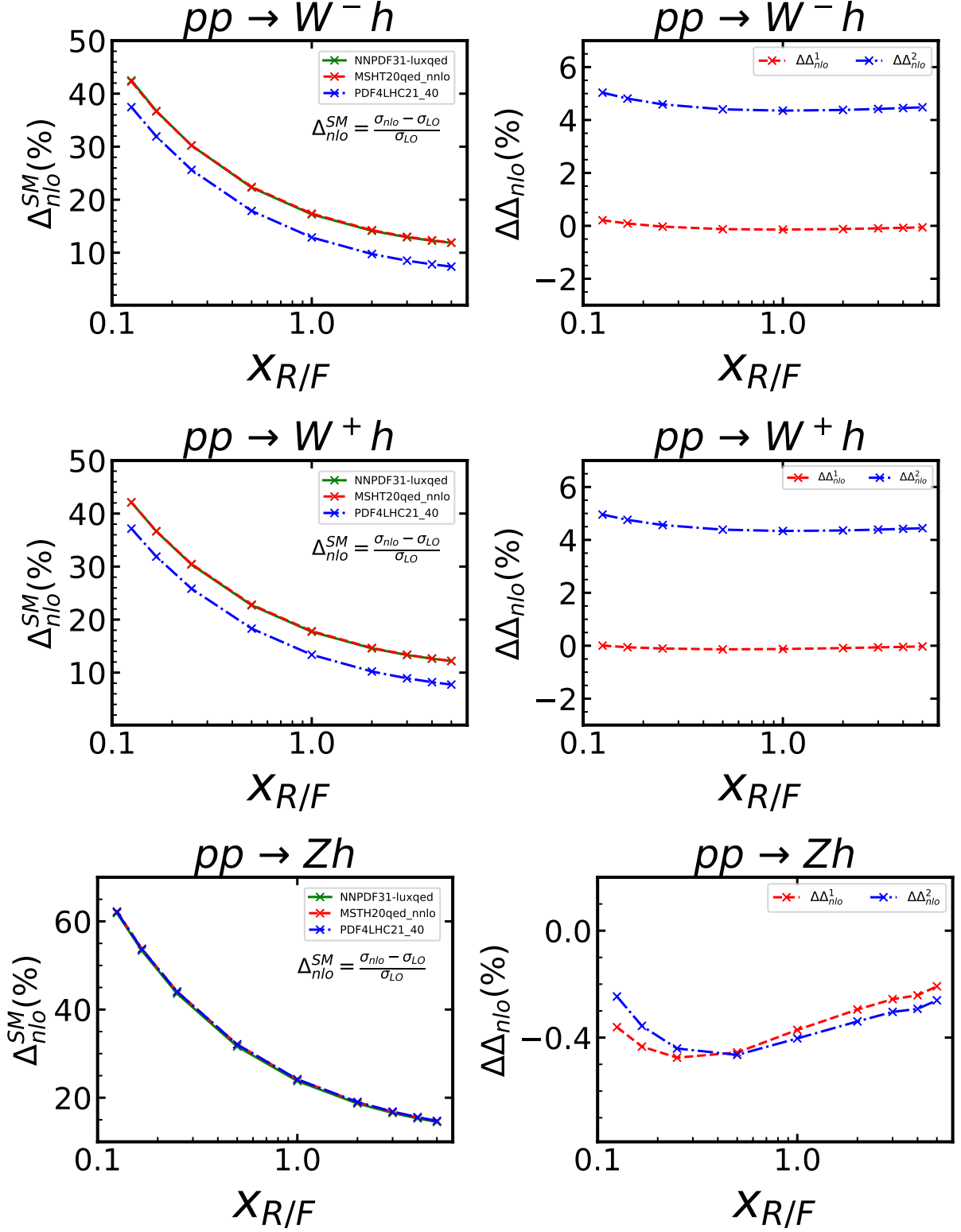


FIG. 17: As in Fig. 8 but for the full NLO, combined QCD and EW corrections for  $Vh$ . The panels on the right gives the difference in the percentage NLO correction taking the NNPDF-1ux as the default PDFs set.

Adding the QCD and the electroweak corrections, the corresponding relative error is displayed in Fig. 17. The important lesson is that in contrast to the NLO QCD corrections, the scale uncertainty of the electroweak corrections that is introduced through convolution of the PDF's (for all three sets of the PDFs) is, as expected, very tiny (at the per-mil level or even better). For the  $Zh$  channel the results of the convolution with all three PDF's agree extremely well (agreement at the per-mil level). As expected the PDFs uncertainty within PDF4LHC21 is smallest. With about  $-5\%$  relative correction for  $Zh$ , we recover here the results of [142] for  $M_h = 125$  GeV. For the full corrections, the PDFs uncertainty is at per-mil level also and is totally negligible for  $x_{R/F} > 1$ , in particular for  $x_{R/F} = 2$  that we have advocated.

For  $W^\pm h$ , the electroweak corrections show important differences beyond the inherent (very tiny) PDFs uncertainty within each set. It is the most precise PDF4LHC21\_40 which disagrees with NNPDF31-luxqed and MSHT20qed\_nnlo, the latter two agreeing extremely well with each other. This is due to the photon induced process whose contribution accounts for the almost 5% difference. As remarked previously this contribution is tiny in the  $Zh$  channel but no so in the  $Wh$  channel. As we underlined previously the spin-1  $W$   $t$ -channel exchange in  $\gamma q \rightarrow Whq'$  is large. We underline also that our results agree extremely well with those of the original calculation of the electroweak corrections in  $Vh$  conducted in [142] when the induced photon contribution is switched off. Considering that the agreement between the results of convoluting with these 3 PDFs was at per-mil level for the QCD correction, the discrepancy in the NLO electroweak correction is due essentially to the contribution of the parameterisation (or lack of) the photon content as seen in Fig. 17. To quantitatively substantiate the argument made earlier that a  $p_T^W$  cut would reduce the contribution of the induced photon cross section,  $\sigma_{\gamma\text{-induced}}$ , Table IV gives the relative size of this contribution (with NNPDF31-luxqed) with increasing  $p_T^W$  cuts. This confirms our argument. This also may explain why  $\sigma_{\gamma\text{-induced}}$  in  $Wh$  has been found to be of order the percent in [143, 145], albeit with an older set of PDFs.

	no cut	$p_T^W > 20$ GeV	$p_T^W > 100$ GeV	$p_T^W > 200$ GeV
$W^-h$	4.5%	4.5%	2.3%	0.9%
$W^+h$	4.5%	4.5%	2.3%	1%

TABLE IV:  $\sigma_{\gamma\text{-induced}}/\sigma_{\text{LO}}$  for different values of the cut on  $p_T^W$  for  $W^\pm h$  production. The NNPDF31-luxqed set is used for the LHC at 13 TeV

Any potential deviation from the SM prediction should therefore be analysed in view of the uncertainties we have discussed. This discussion was based on NLO results (and LO for  $gg \rightarrow Zh$ ). Taking the recent analysis based on  $\text{N}^3\text{LO}$  where estimates for the uncertainties are given (scale variation, PDFs, correlation of the latter), as well as the results [148–152] for higher orders for  $gg \rightarrow Zh$  the present yardstick for the QCD accuracy (for the inclusive cross sections) is just below 2% uncertainty for  $Wh$  and we will take a 2.5% for  $Zh$  which is dominated by the PDFs uncertainty. These PDFs uncertainties should be reduced in the future in particular by improving the extraction of the  $\text{N}^3\text{LO}$  PDFs together with the extraction of their photon component. It is in this light that we should view any deviation from the SM prediction of these cross sections as would be the case of the indirect effects of the IDM to which we now turn.

#### IV. HIGGS-STRAHLUNG IN THE IDM: ONE LOOP RESULTS AND DEVIATIONS FROM THE SM

The IDM does not change any of the couplings that enter the tree-level amplitudes for  $Vh$  production, any effect is therefore *indirect* and appears beyond tree-level. The IDM does not add any new coloured particle, the QCD corrections (virtual and real) are exactly the same as in the SM. The electroweak corrections for  $pp \rightarrow Vh$ , on the other hand, are sensitive to the virtual loop effects of the new scalars (in two-point and three-point functions), without affecting the infra-red/collinear structure. The complete set of the electroweak corrections due to the IDM is displayed in Fig. 18.

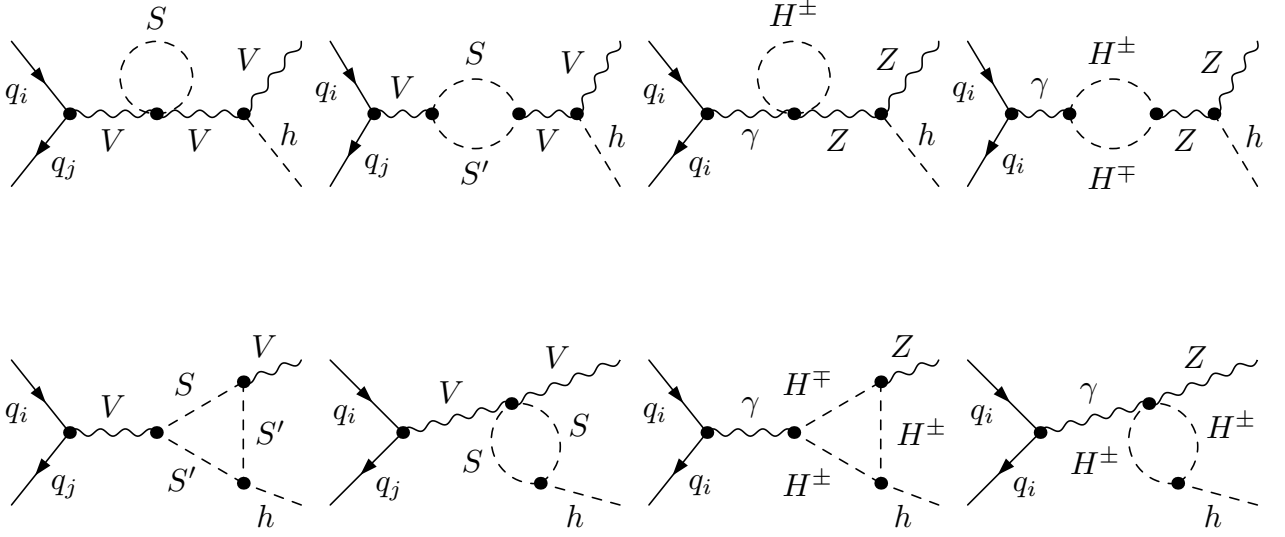


FIG. 18: Additional contributions from the IDM for  $Vh$  production,  $V = Z, W^\pm$ .  $S = H^\pm, X, A$ .  $Zh$  production has additional contributions from  $\gamma - Z$  mixing compared to  $W^\pm h$  production. Diagrams with Goldstone bosons are not shown in this list.

Note that the contribution of the new scalars also enters in the renormalisation of the electroweak sector. As an example the 2-point functions that enter the definition of  $\Delta r$  Eq. 34 also include now the contributions of the new scalars. In this respect it is important to recall that the  $S, T, U$  parameters also constrain the two-point functions contributions involved in  $Vh$  production. A variation of the three-point functions are also constrained from  $h \rightarrow \gamma\gamma$ . This is the reason it is worth investigating how much additional sensitivity  $pp \rightarrow Vh$  production has on the parameters of the IDM once all the constraints are imposed.

Potentially there are also new contributions of the charged scalars of the IDM from  $\gamma\gamma$  induced processes as depicted in Fig. 19. We find that these  $\gamma\gamma$  induced contributions are totally negligible and are in fact much smaller than the SM  $\gamma\gamma$  induced contributions of the SM, which are themselves too tiny.

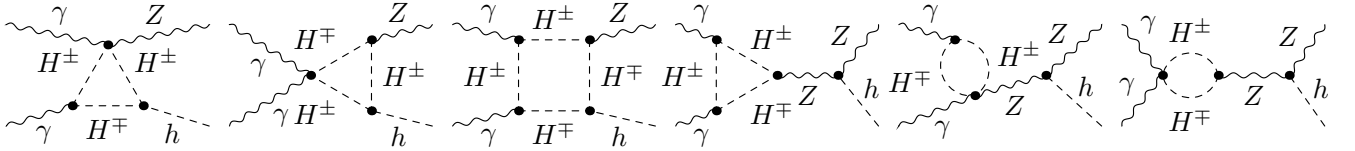


FIG. 19: Feynman diagrams of  $\gamma\gamma \rightarrow Zh$  including the contributions of charged Higgs.

At the end of the day the departure from the SM prediction amounts to the discrepancy in the electroweak virtual corrections to the  $q\bar{q}$  sub-processes between the IDM and the SM. We quantify the percentage change through the variable  $\delta$ ,

$$\delta = \frac{\sigma_{IDM}^{NLO} - \sigma_{SM}^{NLO}}{\sigma_{SM}^{LO}} = \frac{\sigma_{IDM}^{virt-EW} - \sigma_{SM}^{virt-EW}}{\sigma_{SM}^{LO}}. \quad (35)$$

#### A. Scenarios without DM constraints

Taking all the constraints without assuming the model provides a dark matter candidate we have evaluated the deviation  $\delta$ , in all three inclusive cross sections, by scanning over a large scan of the IDM parameters. Our results are displayed in Fig. 20 for two large classes

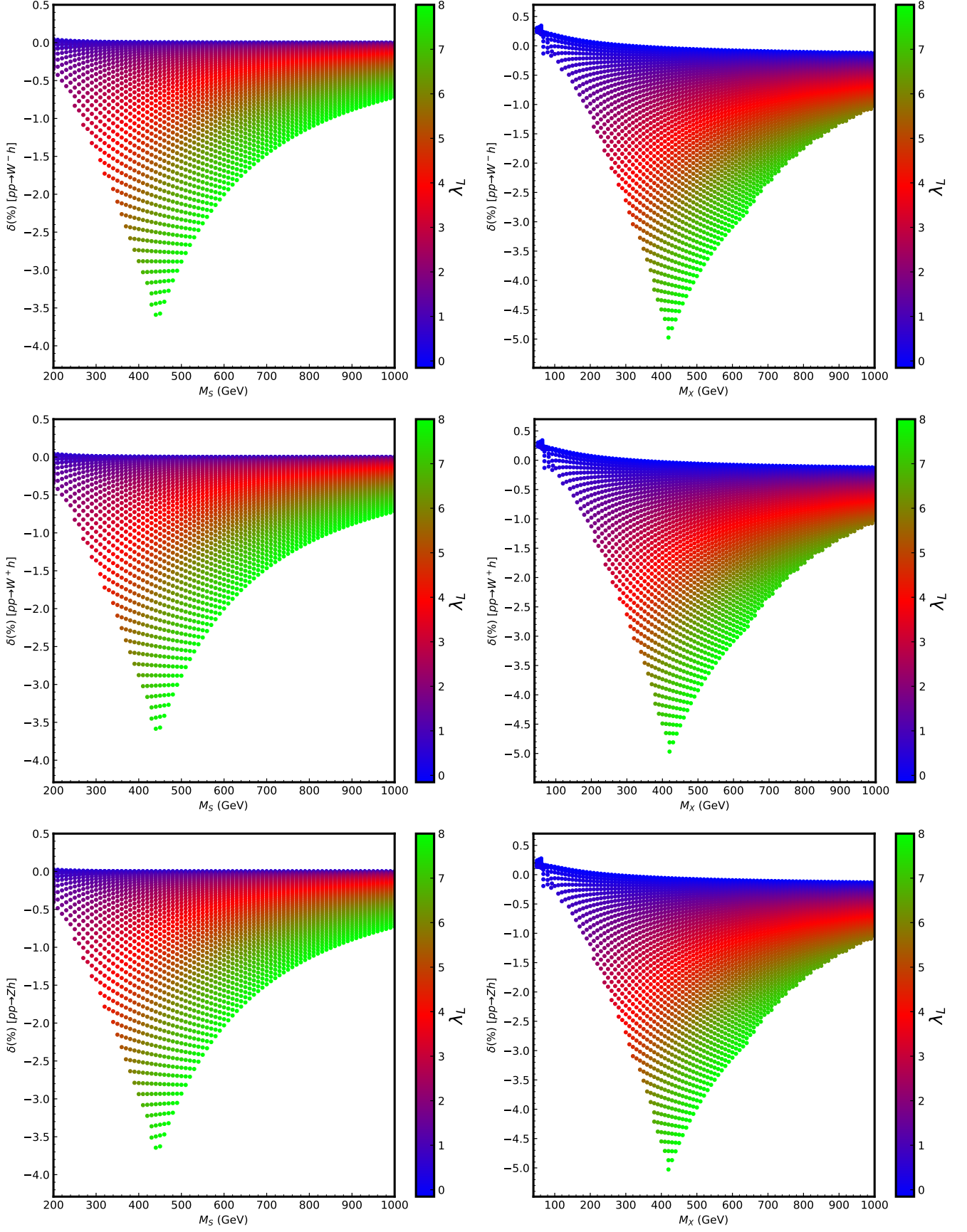


FIG. 20: The percentage difference between the SM and the IDM for  $pp \rightarrow Vh$  cross sections when no DM constraints are imposed but all other constraints are taken into account (see section II B). In the panel on the left there is full degeneracy on the masses of the three extra scalars of the IDM:  $M_X = M_A = M_{H^\pm} = M_S$  (models **A**, see text). In the panel on the right we have  $M_A = M_{H^\pm}$  (models **B**) the mass of the lightest (neutral scalar)  $X$  is taken such that  $\Delta M = M_A - M_X = 100$  GeV. BP0 is not representative of these two scenarios. BP1 belongs to the panel on the left whereas BP2 belongs to the panel on the right.  $\sqrt{s} = 13$  TeV.

- **A:** In this category we consider models with exact degeneracy in the scalar sector:  $M_X = M_A = M_{H^\pm} = M_S$  and scan on  $M_S/M_X$ . In this case we have that  $\lambda_L = \lambda_3 = \lambda_A$ .
- **B:** In this category to which belong BP1 and BP2  $M_A = M_{H^\pm}$ ,  $\Delta M = M_A - M_X = 100$  GeV is kept constant. The scan is over  $M_X$ . In this category  $\lambda_A = \lambda_3$  and  $\lambda_A > \lambda_L$ , the difference between  $\lambda_A$  and  $\lambda_L$  increases as  $M_X$  increases. This means that for the same  $\lambda_L$  in models **A**,  $\lambda_{A,3}$  (couplings to  $hAA, hH^\pm H^\mp$ ) can be larger, and hence we would expect larger deviations.

The most important observation is that deviations larger than  $|\delta| = 2\%$  (above the uncertainty we have set in the SM predictions) are possible in a non negligible part of the parameter space. The largest deviations occur for  $400 < M_X < 500$  GeV, this maximum deviation can be understood on the basis that larger masses make the couplings larger but for too large masses some decoupling takes place. As expected the largest deviations occur with models **B**) reaching values around  $-5\%$  (at  $M_X = 420$  GeV for  $Zh$ ) to maxima around  $-3.5\%$  in models **A** (the all degenerate case). Observe that a characteristic of the IDM is that  $\delta$  is negative throughout the parameter space and is sensibly the same in the 3 processes. Another important observation is that the largest deviations correspond to largest values of  $\lambda_L$ ,  $6 < \lambda_L < 8$ .

Benchmark points BP1 and BP2 of Table I do belong to category **A**. With deviations in  $Zh, W^-h, W^+h$  respectively in BP1 and BP2, BP1 would pass the observability limit in  $W^\pm$  (but not  $Zh$ ) whereas the effects of BP2 would not be resolved. BP0 with deviations reaching almost  $-6\%$  in all channels ( $-5.82\%, -5.76\%, -5.76\%$  in  $Zh, W^-h, W^+h$ ) would be detected in all three channels.

As expected, the normalised ratio  $\delta$  is practically insensitive to the factorization/renormalization scale  $\mu_{R/F}$  in all three channels and for all three benchmarks, as Fig. 21 shows.

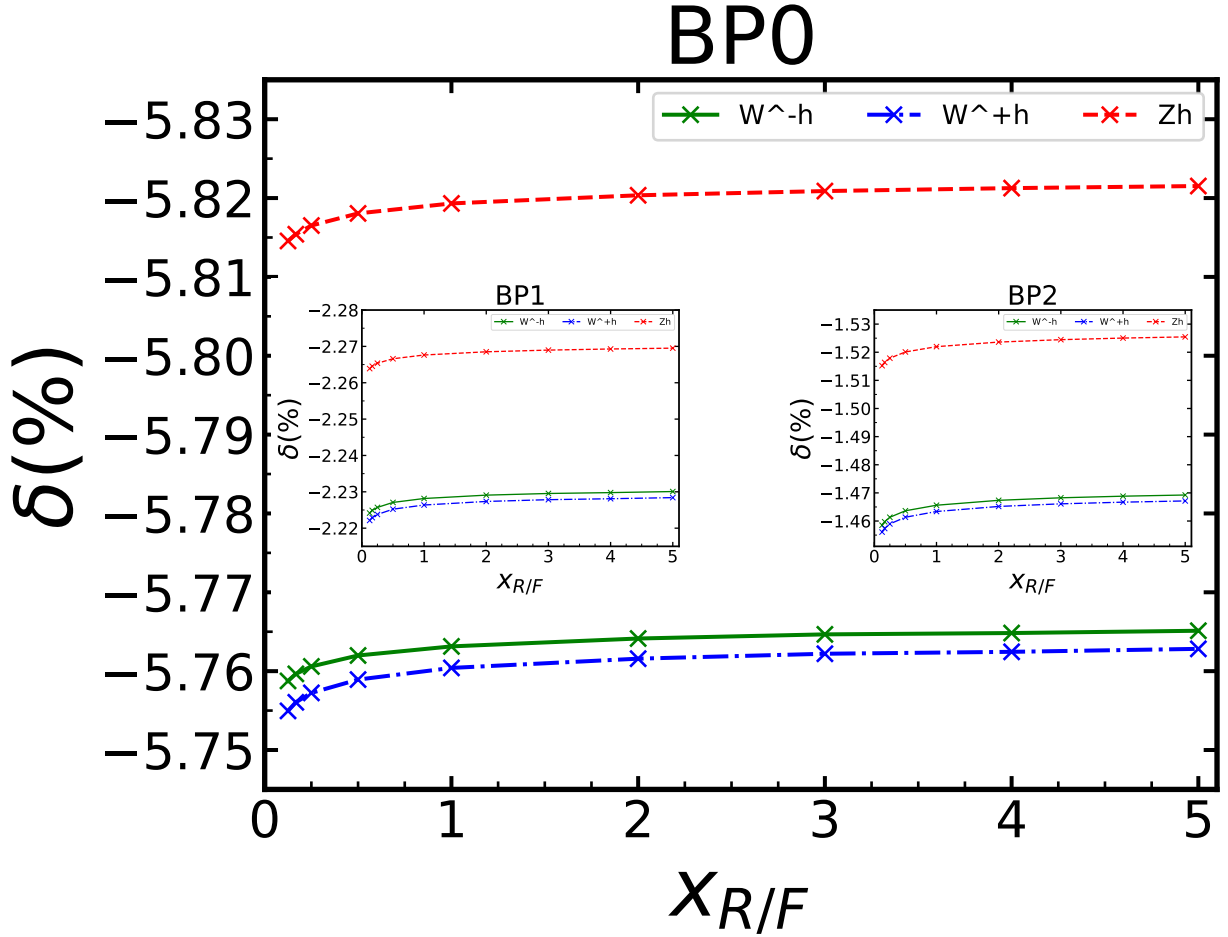


FIG. 21: The  $\mu_{R/F}$  dependence of the normalised relative correction  $\delta$  for benchmark point BP0 for the three Higgs-strahlung processes. The  $\mu_{R/F}$  dependence is tracked through the variable  $x_{R/F}$ , see Eq. 30. The inserts correspond to BP1 (left) and BP2 (right).

We have also analysed whether the shifts from the SM in the total cross sections manifest themselves through characteristic distributions that would further help in distinguishing the IDM. We have analysed the transverse momentum and rapidity distributions of the Higgs  $h$  for the three benchmark points BP0, BP1 and BP2. We find that, independently which of the three cross sections or the benchmark point is considered, the shifts in the cross sections are practically equally distributed particularly for  $p_T^h$ , whereas there is clearly an distinctive structure for the  $p_T^h$  distribution from the electroweak correction within the SM, see Fig 22. For the rapidity distribution,  $y^h$ , the SM electroweak corrections are revealed through a quite distinctive feature, both for  $W^\pm h$  and  $Zh$  particularly around large  $|y^h|$ . The added effect of the IDM is not as subtle as on the  $p_T^h$  distribution with a small disturbance from the SM results affecting central events around  $y \sim 0$ . Note however that these are the regions where the cross sections are smallest, see Fig. 23. The effect may therefore not be resolved.

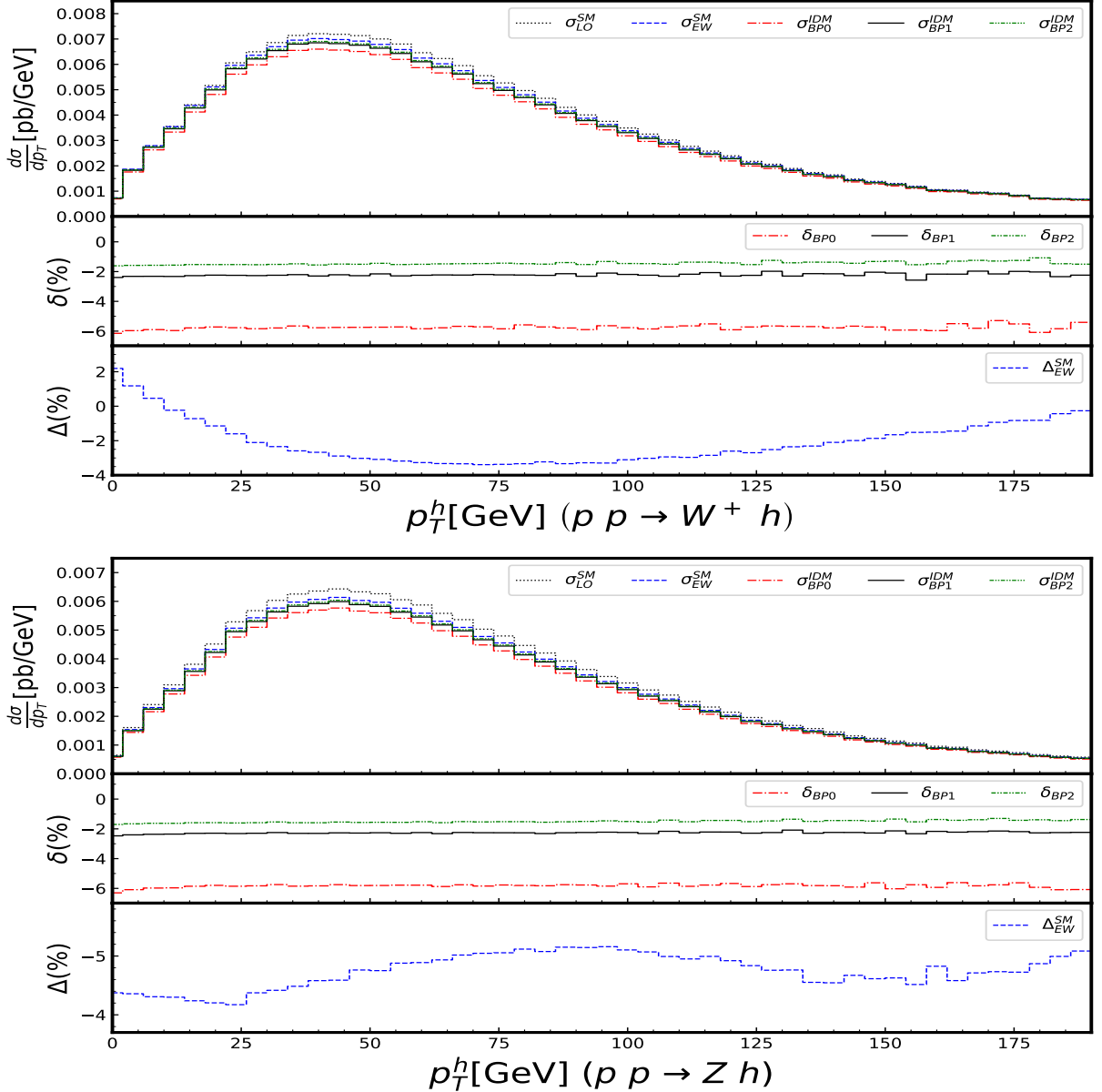
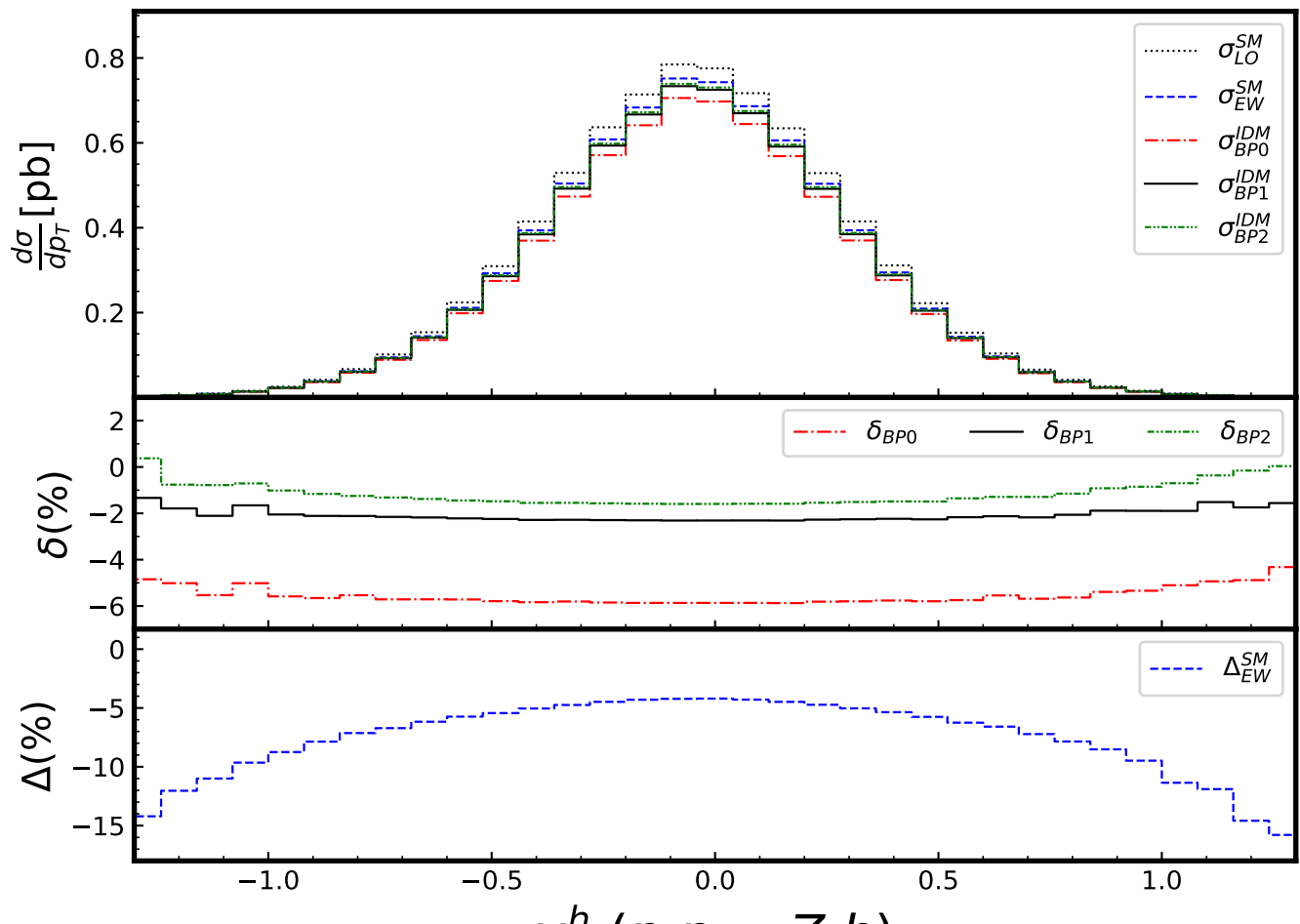
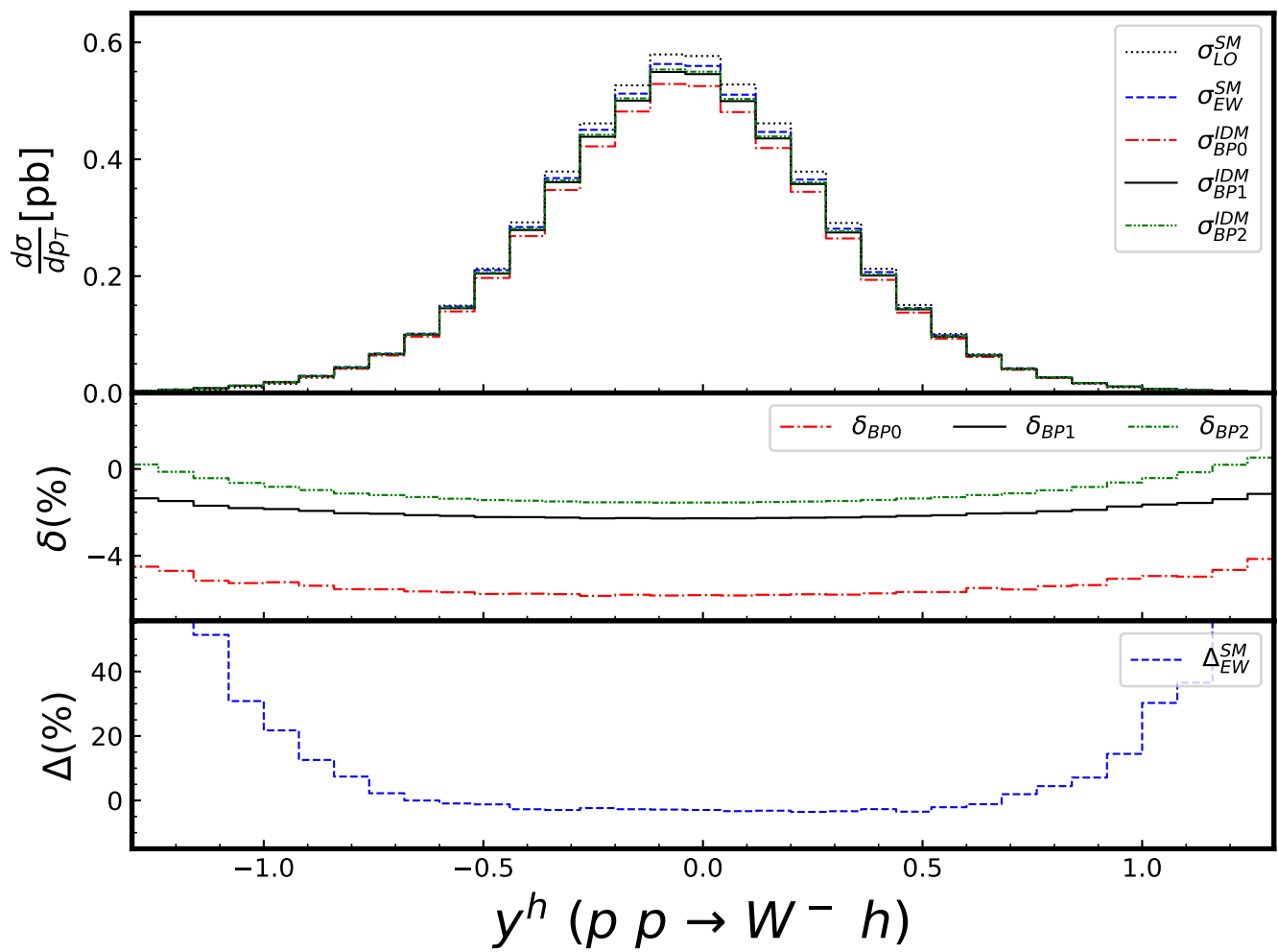


FIG. 22: We take two illustrative examples ( $W^+h$  and  $Zh$  channels) the impact of the new scalars on the  $p_T^h$  distribution. The LO(black dots line), SM EW(blue dashed line) and IDM EW(red dots and dashed line for BP0, black line for BP1 and green dots and dashed for BP2) at 13TeV LHC. The percentage shift  $\delta$  for the distributions is shown in the panel below each distribution. In the panel on the bottom we show the percentage correction for the SM electroweak correction,  $\Delta \equiv \Delta_{EW}^{SM} = (\frac{d\sigma_{EW}^{SM}}{dp_T^h} - \frac{d\sigma_{LO}^{SM}}{dp_T^h}) / \frac{d\sigma_{LO}^{SM}}{dp_T^h}$ .



### B. Scenarios with DM constraints

We now impose the DM constraints. As pointed earlier, direct detection requires extremely small values for  $\lambda_L$ ,  $\lambda_L$  of order the percent or smaller. For not too large spectrum and to conform with custodial symmetry, the other couplings  $\lambda_3, \lambda_A$  are smaller than 1, see section II B. The results of the scan in Fig. 20 give us an indication on the expected deviation  $\delta$  in these scenarios. The deviations for small  $\lambda_L < 1$  are extremely small,  $|\delta| < 0.5\%$  (see Fig. 20). This is confirmed by the analysis of the benchmark points BP3-BP5 as Table V shows (the results are essentially the same for the LHC at 14 TeV). The deviations when the DM constraints are taken into account are at best at the per-mil level, this is in  $W^\pm h$   $\delta$  for BP4 (this is understood on the basis that this BP has the largest coupling  $\lambda_3 = \lambda_{hAA}$  combined with the smallest value of the neutral scalar  $A$ ). Even in this most favourable situation the deviation is below 0.4%. When DM constraints come into play the effect of the IDM in precision indirect effects of  $pp \rightarrow Vh$  cross sections at the LHC are not observable.

	BP3	BP4	BP5
$Zh$	0.07	$\mathcal{O}(10^{-3})$	$-\mathcal{O}(10^{-3})$
$W^-h$	0.20	0.35	$-\mathcal{O}(10^{-3})$
$W^+h$	0.19	0.34	$-\mathcal{O}(10^{-3})$

TABLE V: The deviation  $\delta$  in % for the benchmark points BP3, BP4 and BP5 (with dark matter constraints imposed) on the  $Vh$  cross sections at the 13 TeV LHC.

### V. SUMMARY

Higgs-strahlung processes at the LHC are entering the era of precision measurements (computations of N<sup>3</sup>LO QCD are among the latest achievements [139]) while the accuracy of the PDFs has greatly improved. Such processes are therefore prime observables to investigate indirect, virtual effects of New Physics. In the present study we considered the effects of the IDM. The indirect effects of the latter are electroweak in essence. One of the purpose of the study, which is part of a more extensive goal, is to develop a general tool to perform one-loop calculations at the LHC in beyond SM theories, a tool which can, on the one hand, tackle both NLO QCD and one-loop electroweak corrections and allows to cover both scale and PDFs uncertainties in the SM calculations and, on the other hand, precisely compute the effects of models of New Physics within the same framework. We have shown that initiated  $\gamma q \rightarrow W^\pm h$  production can be non negligible in the calculation of the inclusive cross sections, even if a  $p_T^W$  cut can reduce this contribution. The main motivation for the study was also to answer the question whether once the constraints, such EWPO (Electroweak Precision Observables), non observation of the physical states of the model, limits on the partial widths of the Higgs still allow for the possible future observation of deviations in any of the three processes ( $W^\pm h, Zh$ ) at the LHC. The answer is that deviations in the total yield are indeed possible, even after taking into account the PDFs and parametric uncertainties of the SM cross sections. In general, deviations are found in both the charged and neutral channel. Unfortunately, no clear discernible structure is found in the distributions  $(p_T^h, y_h)$  we looked at. When the IDM is elevated to a model that provides a possible dark matter candidate and that constraints are imposed from the dark matter sector, in particular direct detection, the model becomes so constrained that deviations in precision measurements in all Higgs-strahlung processes are too minuscule to observe.

### Acknowledgments

H.S. is supported by the National Natural Science Foundation of China under Grants No. 12075043. Y.Z. is supported by the National Natural Science Foundation of China under Grant No. 11805001 and the Fundamental Research Funds for the Central Universities under Grant No. JZ2023HG TB0222. We thank Jean-Philippe Guillet for

discussions and a careful reading of the manuscript.

- 
- [1] G. Aad et al. (ATLAS), Phys. Lett. B **716**, 1 (2012), 1207.7214.
  - [2] S. Chatrchyan et al. (CMS), Phys. Lett. B **716**, 30 (2012), 1207.7235.
  - [3] N. G. Deshpande and E. Ma, Phys. Rev. **D18**, 2574 (1978).
  - [4] R. Barbieri, L. J. Hall, and V. S. Rychkov, Phys. Rev. **D74**, 015007 (2006), hep-ph/0603188.
  - [5] T. Hambye and M. H. G. Tytgat, Phys. Lett. **B659**, 651 (2008), 0707.0633.
  - [6] S. Kanemura, S. Kiyoura, Y. Okada, E. Senaha, and C. P. Yuan, Phys. Lett. B **558**, 157 (2003), hep-ph/0211308.
  - [7] L. Lopez Honorez, E. Nezri, J. F. Oliver, and M. H. G. Tytgat, JCAP **0702**, 028 (2007), hep-ph/0612275.
  - [8] Q.-H. Cao, E. Ma, and G. Rajasekaran, Phys. Rev. D **76**, 095011 (2007), 0708.2939.
  - [9] M. Gustafsson, E. Lundstrom, L. Bergstrom, and J. Edsjo, Phys. Rev. Lett. **99**, 041301 (2007), astro-ph/0703512.
  - [10] P. Agrawal, E. M. Dolle, and C. A. Krenke, Phys. Rev. **D79**, 015015 (2009), 0811.1798.
  - [11] E. Lundstrom, M. Gustafsson, and J. Edsjo, Phys. Rev. D **79**, 035013 (2009), 0810.3924.
  - [12] T. Hambye, F. S. Ling, L. Lopez Honorez, and J. Rocher, JHEP **07**, 090 (2009), [Erratum: JHEP **05**, 066 (2010)], 0903.4010.
  - [13] S. Andreas, M. H. G. Tytgat, and Q. Swillens, JCAP **0904**, 004 (2009), 0901.1750.
  - [14] C. Arina, F.-S. Ling, and M. H. G. Tytgat, JCAP **0910**, 018 (2009), 0907.0430.
  - [15] E. Dolle, X. Miao, S. Su, and B. Thomas, Phys. Rev. D **81**, 035003 (2010), 0909.3094.
  - [16] E. Nezri, M. H. G. Tytgat, and G. Vertongen, JCAP **0904**, 014 (2009), 0901.2556.
  - [17] P. M. Ferreira and D. R. T. Jones, JHEP **08**, 069 (2009), 0903.2856.
  - [18] X. Miao, S. Su, and B. Thomas, Phys. Rev. D **82**, 035009 (2010), 1005.0090.
  - [19] J.-O. Gong, H. M. Lee, and S. K. Kang, JHEP **04**, 128 (2012), 1202.0288.
  - [20] M. Gustafsson, S. Rydbeck, L. Lopez-Honorez, and E. Lundstrom, Phys. Rev. D **86**, 075019 (2012), 1206.6316.
  - [21] B. Swiezewska and M. Krawczyk, Phys. Rev. D **88**, 035019 (2013), 1212.4100.
  - [22] L. Wang and X.-F. Han, JHEP **05**, 088 (2012), 1203.4477.
  - [23] A. Arhrib, R. Benbrik, and N. Gaur, Phys. Rev. D **85**, 095021 (2012), 1201.2644.
  - [24] M. Klasen, C. E. Yaguna, and J. D. Ruiz-Alvarez, Phys. Rev. D **87**, 075025 (2013), 1302.1657.
  - [25] M. Aoki, S. Kanemura, and H. Yokoya, Phys. Lett. B **725**, 302 (2013), 1303.6191.
  - [26] S.-Y. Ho and J. Tandean, Phys. Rev. D **89**, 114025 (2014), 1312.0931.
  - [27] A. Goudelis, B. Herrmann, and O. Stål, JHEP **09**, 106 (2013), 1303.3010.
  - [28] A. Arhrib, Y.-L. S. Tsai, Q. Yuan, and T.-C. Yuan, JCAP **06**, 030 (2014), 1310.0358.
  - [29] M. Krawczyk, D. Sokolowska, P. Swaczyna, and B. Swiezewska, JHEP **09**, 055 (2013), 1305.6266.
  - [30] P. Osland, A. Pukhov, G. M. Pruna, and M. Purmohammadi, JHEP **04**, 040 (2013), 1302.3713.
  - [31] I. F. Ginzburg, J. Mod. Phys. **5**, 1036 (2014), 1410.0869.
  - [32] T. Abe and R. Sato, JHEP **03**, 109 (2015), 1501.04161.
  - [33] A. Arhrib, R. Benbrik, J. El Falaki, and A. Jueid, JHEP **12**, 007 (2015), 1507.03630.
  - [34] N. Blinov, J. Kozaczuk, D. E. Morrissey, and A. de la Puente, Phys. Rev. D **93**, 035020 (2016), 1510.08069.
  - [35] M. A. Díaz, B. Koch, and S. Urrutia-Quiroga, Adv. High Energy Phys. **2016**, 8278375 (2016), 1511.04429.
  - [36] A. Ilnicka, M. Krawczyk, and T. Robens, Phys. Rev. D **93**, 055026 (2016), 1508.01671.
  - [37] G. Belanger, B. Dumont, A. Goudelis, B. Herrmann, S. Kraml, and D. Sengupta, Phys. Rev. D **91**, 115011 (2015), 1503.07367.
  - [38] A. Carmona and M. Chala, JHEP **06**, 105 (2015), 1504.00332.
  - [39] F. S. Queiroz and C. E. Yaguna, JCAP **02**, 038 (2016), 1511.05967.
  - [40] P. M. Ferreira and B. Swiezewska, JHEP **04**, 099 (2016), 1511.02879.
  - [41] C. Garcia-Cely, M. Gustafsson, and A. Ibarra, JCAP **02**, 043 (2016), 1512.02801.
  - [42] M. Hashemi, M. Krawczyk, S. Najjari, and A. F. Żarnecki, JHEP **02**, 187 (2016), 1512.01175.
  - [43] A. Datta, N. Ganguly, N. Khan, and S. Rakshit, Phys. Rev. D **95**, 015017 (2017), 1610.00648.
  - [44] A. G. Akeroyd et al., Eur. Phys. J. C **77**, 276 (2017), 1607.01320.
  - [45] S. Kanemura, M. Kikuchi, and K. Sakurai, Phys. Rev. D **94**, 115011 (2016), 1605.08520.
  - [46] A. Belyaev, G. Cacciapaglia, I. P. Ivanov, F. Rojas-Abatte, and M. Thomas, Phys. Rev. D **97**, 035011 (2018), 1612.00511.
  - [47] S. Banerjee and N. Chakrabarty, JHEP **05**, 150 (2019), 1612.01973.
  - [48] P. Poullose, S. Sahoo, and K. Sridhar, Phys. Lett. B **765**, 300 (2017), 1604.03045.
  - [49] B. Eiteneuer, A. Goudelis, and J. Heisig, Eur. Phys. J. C **77**, 624 (2017), 1705.01458.
  - [50] E. Senaha, Phys. Rev. D **100**, 055034 (2019), 1811.00336.
  - [51] A. Ilnicka, T. Robens, and T. Stefaniak, Mod. Phys. Lett. A **33**, 1830007 (2018), 1803.03594.
  - [52] J. Kalinowski, W. Kotlarski, T. Robens, D. Sokolowska, and A. F. Żarnecki, JHEP **12**, 081 (2018), 1809.07712.
  - [53] G. Arcadi, A. Djouadi, and M. Raidal, Phys. Rept. **842**, 1 (2020), 1903.03616.
  - [54] J. Braathen and S. Kanemura, Phys. Lett. B **796**, 38 (2019), 1903.05417.
  - [55] S. Banerjee, F. Boudjema, N. Chakrabarty, G. Chalons, and H. Sun, Phys. Rev. D **100**, 095024 (2019), 1906.11269.
  - [56] A. Bhardwaj, P. Konar, T. Mandal, and S. Sadhukhan, Phys. Rev. D **100**, 055040 (2019), 1905.04195.
  - [57] A. F. Żarnecki, J. Kalinowski, J. Klamka, P. Sopicki, W. Kotlarski, T. Robens, and D. Sokolowska, PoS **ALPS2019**, 010 (2020), 1908.04659.

- [58] D. Sokolowska, J. Kalinowski, J. Klamka, P. Sopicki, A. F. Zarnecki, W. Kotlarski, and T. Robens, PoS **EPS-HEP2019**, 570 (2020), 1911.06254.
- [59] R. Basu, S. Banerjee, M. Pandey, and D. Majumdar (2020), 2010.11007.
- [60] H. Abouabid, A. Arhrib, R. Benbrik, J. El Falaki, B. Gong, W. Xie, and Q.-S. Yan, JHEP **05**, 100 (2021), 2009.03250.
- [61] A. F. Zarnecki, J. Kalinowski, J. Klamka, P. Sopicki, W. Kotlarski, T. Robens, and D. Sokolowska, in *International Workshop on Future Linear Colliders* (2020), 2002.11716.
- [62] A. F. Zarnecki, J. Kalinowski, J. Klamka, P. Sopicki, W. Kotlarski, T. N. Robens, and D. Sokolowska, PoS **CORFU2019**, 047 (2020).
- [63] J. Kalinowski, T. Robens, D. Sokolowska, and A. F. Zarnecki, Symmetry **13**, 991 (2021), 2012.14818.
- [64] S. Banerjee, F. Boudjema, N. Chakrabarty, and H. Sun, Phys. Rev. D **104**, 075002 (2021), 2101.02165.
- [65] S. Banerjee, F. Boudjema, N. Chakrabarty, and H. Sun, Phys. Rev. D **104**, 075003 (2021), 2101.02166.
- [66] S. Banerjee, F. Boudjema, N. Chakrabarty, and H. Sun, Phys. Rev. D **104**, 075004 (2021), 2101.02167.
- [67] S. Banerjee, F. Boudjema, N. Chakrabarty, and H. Sun, Phys. Rev. D **104**, 075005 (2021), 2101.02170.
- [68] T. Robens, in *55th Rencontres de Moriond on QCD and High Energy Interactions* (2021), 2105.07719.
- [69] T. Robens, J. Kalinowski, A. F. Zarnecki, and A. Papaefstathiou, Acta Phys. Polon. B **52**, 1055 (2021), 2104.00046.
- [70] T. Robens, PoS **EPS-HEP2021**, 715 (2022), 2110.07294.
- [71] M. J. Ramsey-Musolf, J.-H. Yu, and J. Zhou, JHEP **10**, 155 (2021), 2104.10709.
- [72] A. Ghosh, P. Konar, and S. Seth, Phys. Rev. D **105**, 115038 (2022), 2111.15236.
- [73] M. Aiko, S. Kanemura, and K. Mawatari, Eur. Phys. J. C **81**, 1000 (2021), 2109.02884.
- [74] M. Aiko, Ph.D. thesis, Osaka U. (2022).
- [75] H. Abouabid, A. Arhrib, J. E. Falaki, B. Gong, W. Xie, and Q.-S. Yan (2022), 2204.05237.
- [76] J. Alwall, R. Frederix, S. Frixione, V. Hirschi, F. Maltoni, O. Mattelaer, H. S. Shao, T. Stelzer, P. Torrielli, and M. Zaro, JHEP **07**, 079 (2014), 1405.0301.
- [77] F. Boudjema, A. Semenov, and D. Temes, Phys. Rev. D **72**, 055024 (2005), hep-ph/0507127.
- [78] N. Baro, F. Boudjema, and A. Semenov, Phys. Lett. B **660**, 550 (2008), 0710.1821.
- [79] N. Baro, F. Boudjema, and A. Semenov, Phys. Rev. D **78**, 115003 (2008), 0807.4668.
- [80] N. Baro, F. Boudjema, G. Chalons, and S. Hao, Phys. Rev. D **81**, 015005 (2010), 0910.3293.
- [81] F. Boudjema, G. Drieu La Rochelle, and S. Kulkarni, Phys. Rev. D **84**, 116001 (2011), 1108.4291.
- [82] F. Boudjema, G. Drieu La Rochelle, and A. Mariano, Phys. Rev. D **89**, 115020 (2014), 1403.7459.
- [83] G. Belanger, V. Bizouard, F. Boudjema, and G. Chalons, Phys. Rev. D **93**, 115031 (2016), 1602.05495.
- [84] G. Bélanger, V. Bizouard, F. Boudjema, and G. Chalons, Phys. Rev. D **96**, 015040 (2017), 1705.02209.
- [85] S. Catani and M. H. Seymour, Phys. Lett. B **378**, 287 (1996), hep-ph/9602277.
- [86] S. Catani and M. H. Seymour, Nucl. Phys. B **485**, 291 (1997), [Erratum: Nucl.Phys.B 510, 503–504 (1998)], hep-ph/9605323.
- [87] S. Catani, S. Dittmaier, M. H. Seymour, and Z. Trocsanyi, Nucl. Phys. B **627**, 189 (2002), hep-ph/0201036.
- [88] B. W. Harris and J. F. Owens, Phys. Rev. D **65**, 094032 (2002), hep-ph/0102128.
- [89] G. C. Branco, P. M. Ferreira, L. Lavoura, M. N. Rebelo, M. Sher, and J. P. Silva, Phys. Rept. **516**, 1 (2012), 1106.0034.
- [90] B. W. Lee, C. Quigg, and H. B. Thacker, Phys. Rev. D **16**, 1519 (1977).
- [91] M. E. Peskin and T. Takeuchi, Phys. Rev. D **46**, 381 (1992).
- [92] M. Baak, M. Goebel, J. Haller, A. Hoecker, D. Kennedy, K. Moenig, M. Schott, and J. Stelzer (Gfitter), Eur. Phys. J. C **72**, 2003 (2012), 1107.0975.
- [93] Y.-L. S. Tsai, V. Q. Tran, and C.-T. Lu, JHEP **06**, 033 (2020), 1912.08875.
- [94] M. Aaboud et al. (ATLAS), JHEP **01**, 126 (2018), 1711.03301.
- [95] G. Aad et al. (ATLAS), Phys. Rev. D **100**, 052013 (2019), 1906.05609.
- [96] G. Aad et al. (ATLAS), Phys. Rev. D **104**, 112010 (2021), 2108.07586.
- [97] A. Djouadi, Phys. Rept. **457**, 1 (2008), hep-ph/0503172.
- [98] M. Aaboud et al. (ATLAS), Phys. Rev. D **98**, 052005 (2018), 1802.04146.
- [99] A. M. Sirunyan et al. (CMS), JHEP **11**, 185 (2018), 1804.02716.
- [100] G. Aad et al. (ATLAS), Phys. Lett. B **842**, 137963 (2023), 2301.10731.
- [101] A. Tumasyan et al. (CMS) (2023), 2303.01214.
- [102] G. Belanger, F. Boudjema, A. Pukhov, and A. Semenov, Comput. Phys. Commun. **149**, 103 (2002), hep-ph/0112278.
- [103] G. Belanger, F. Boudjema, A. Pukhov, and A. Semenov, Comput. Phys. Commun. **174**, 577 (2006), hep-ph/0405253.
- [104] G. Belanger, F. Boudjema, A. Pukhov, and A. Semenov, Comput. Phys. Commun. **176**, 367 (2007), hep-ph/0607059.
- [105] G. Belanger, F. Boudjema, A. Pukhov, and A. Semenov, Comput. Phys. Commun. **185**, 960 (2014), 1305.0237.
- [106] G. Bélanger, F. Boudjema, A. Goudelis, A. Pukhov, and B. Zaldivar, Comput. Phys. Commun. **231**, 173 (2018), 1801.03509.
- [107] J. Aalbers et al. (LZ) (2022), 2207.03764.
- [108] M. Cirelli, N. Fornengo, and A. Strumia, Nucl. Phys. B **753**, 178 (2006), hep-ph/0512090.
- [109] V. D. Barger, E. W. N. Glover, K. Hikasa, W.-Y. Keung, M. G. Olsson, C. J. Suchyta, and X. R. Tata, Phys. Rev. Lett. **57**, 1672 (1986).
- [110] D. A. Dicus and C. Kao, Phys. Rev. D **38**, 1008 (1988), [Erratum: Phys.Rev.D 42, 2412 (1990)].
- [111] B. A. Kniehl, Phys. Rev. D **42**, 2253 (1990).
- [112] T. Han and S. Willenbrock, Phys. Lett. B **273**, 167 (1991).
- [113] J. Ohnemus and W. J. Stirling, Phys. Rev. D **47**, 2722 (1993).
- [114] H. Baer, B. Bailey, and J. F. Owens, Phys. Rev. D **47**, 2730 (1993).
- [115] C. Zecher, T. Matsuura, and J. J. van der Bij, Z. Phys. C **64**, 219 (1994), hep-ph/9404295.

- [116] Q.-H. Cao, C.-S. Li, and S.-H. Zhu, *Commun. Theor. Phys.* **33**, 275 (2000), hep-ph/9810458.
- [117] R. V. Harlander and W. B. Kilgore, *Phys. Rev. Lett.* **88**, 201801 (2002), hep-ph/0201206.
- [118] O. Brein, A. Djouadi, and R. Harlander, *Phys. Lett. B* **579**, 149 (2004), hep-ph/0307206.
- [119] O. Brein, R. Harlander, M. Wiesemann, and T. Zirke, *Eur. Phys. J. C* **72**, 1868 (2012), 1111.0761.
- [120] G. Ferrera, M. Grazzini, and F. Tramontano, *Phys. Rev. Lett.* **107**, 152003 (2011), 1107.1164.
- [121] A. Banfi and J. Cancino, *Phys. Lett. B* **718**, 499 (2012), 1207.0674.
- [122] O. Brein, R. V. Harlander, and T. J. E. Zirke, *Comput. Phys. Commun.* **184**, 998 (2013), 1210.5347.
- [123] L. Altenkamp, S. Dittmaier, R. V. Harlander, H. Rzehak, and T. J. E. Zirke, *JHEP* **02**, 078 (2013), 1211.5015.
- [124] C. Englert, M. McCullough, and M. Spannowsky, *Phys. Rev. D* **89**, 013013 (2014), 1310.4828.
- [125] G. Ferrera, M. Grazzini, and F. Tramontano, *JHEP* **04**, 039 (2014), 1312.1669.
- [126] M. C. Kumar, M. K. Mandal, and V. Ravindran, *JHEP* **03**, 037 (2015), 1412.3357.
- [127] G. Ferrera, M. Grazzini, and F. Tramontano, *Phys. Lett. B* **740**, 51 (2015), 1407.4747.
- [128] B. Hespel, F. Maltoni, and E. Vryonidou, *JHEP* **06**, 065 (2015), 1503.01656.
- [129] J. M. Campbell, R. K. Ellis, and C. Williams, *JHEP* **06**, 179 (2016), 1601.00658.
- [130] A. Hasselhuhn, T. Luthe, and M. Steinhauser, *JHEP* **01**, 073 (2017), 1611.05881.
- [131] F. Caola, G. Luisoni, K. Melnikov, and R. Rötsch, *Phys. Rev. D* **97**, 074022 (2018), 1712.06954.
- [132] G. Ferrera, G. Somogyi, and F. Tramontano, *Phys. Lett. B* **780**, 346 (2018), 1705.10304.
- [133] R. V. Harlander, J. Klappert, S. Liebler, and L. Simon, *Journal of High Energy Physics* **2018** (2018), URL <https://doi.org/10.1007/2Fjhep05%282018%29089>.
- [134] R. Gauld, A. Gehrmann-De Ridder, E. W. N. Glover, A. Huss, and I. Majer, *JHEP* **10**, 002 (2019), 1907.05836.
- [135] I. Majer, Ph.D. thesis, Zurich, ETH, Zurich, ETH (2020).
- [136] G. Heinrich, *Phys. Rept.* **922**, 1 (2021), 2009.00516.
- [137] L. Chen, G. Heinrich, S. P. Jones, M. Kerner, J. Klappert, and J. Schlenk, *JHEP* **03**, 125 (2021), 2011.12325.
- [138] G. Wang, X. Xu, Y. Xu, and L. L. Yang, *Phys. Lett. B* **829**, 137087 (2022), 2107.08206.
- [139] J. Baglio, C. Duhr, B. Mistlberger, and R. Szafron (2022), 2209.06138.
- [140] G. Degrossi, R. Gröber, M. Vitti, and X. Zhao, *JHEP* **08**, 009 (2022), 2205.02769.
- [141] L. Chen, J. Davies, G. Heinrich, S. P. Jones, M. Kerner, G. Mishima, J. Schlenk, and M. Steinhauser, *JHEP* **08**, 056 (2022), 2204.05225.
- [142] M. L. Ciccolini, S. Dittmaier, and M. Kramer, *Phys. Rev. D* **68**, 073003 (2003), hep-ph/0306234.
- [143] A. Denner, S. Dittmaier, S. Kallweit, and A. Muck, *JHEP* **03**, 075 (2012), 1112.5142.
- [144] A. Denner, S. Dittmaier, S. Kallweit, and A. Muck, *PoS EPS-HEP2011*, 235 (2011), 1112.5258.
- [145] A. Denner, S. Dittmaier, S. Kallweit, and A. Mück, *Comput. Phys. Commun.* **195**, 161 (2015), 1412.5390.
- [146] F. Granata, J. M. Lindert, C. Oleari, and S. Pozzorini, *JHEP* **09**, 012 (2017), 1706.03522.
- [147] P. Obul, S. Dulat, T.-J. Hou, A. Tursun, and N. Yalkun, *Chin. Phys. C* **42**, 093105 (2018), 1801.06851.
- [148] J. Davies, G. Mishima, and M. Steinhauser, *Journal of High Energy Physics* **2021** (2021), ISSN 1029-8479, URL [http://dx.doi.org/10.1007/JHEP03\(2021\)034](http://dx.doi.org/10.1007/JHEP03(2021)034).
- [149] L. Chen, G. Heinrich, S. P. Jones, M. Kerner, J. Klappert, and J. Schlenk, *Journal of High Energy Physics* **2021** (2021), ISSN 1029-8479, URL [http://dx.doi.org/10.1007/JHEP03\(2021\)125](http://dx.doi.org/10.1007/JHEP03(2021)125).
- [150] L. Alasfar, G. Degrossi, P. P. Giardino, R. Gröber, and M. Vitti, *Journal of High Energy Physics* **2021** (2021), ISSN 1029-8479, URL [http://dx.doi.org/10.1007/JHEP05\(2021\)168](http://dx.doi.org/10.1007/JHEP05(2021)168).
- [151] G. Wang, X. Xu, Y. Xu, and L. L. Yang, *Physics Letters B* **829**, 137087 (2022), ISSN 0370-2693, URL <http://dx.doi.org/10.1016/j.physletb.2022.137087>.
- [152] L. Chen, J. Davies, G. Heinrich, S. P. Jones, M. Kerner, G. Mishima, J. Schlenk, and M. Steinhauser, *Journal of High Energy Physics* **2022** (2022), ISSN 1029-8479, URL [http://dx.doi.org/10.1007/JHEP08\(2022\)056](http://dx.doi.org/10.1007/JHEP08(2022)056).
- [153] A. Semenov, *Comput. Phys. Commun.* **201**, 167 (2016), 1412.5016.
- [154] A. Semenov (2010), 1005.1909.
- [155] A. Semenov, *Comput. Phys. Commun.* **180**, 431 (2009), 0805.0555.
- [156] A. V. Semenov (2002), hep-ph/0208011.
- [157] A. Semenov, *Comput. Phys. Commun.* **115**, 124 (1998).
- [158] A. V. Semenov (1996), hep-ph/9608488.
- [159] J. Kublbeck, M. Bohm, and A. Denner, *Comput. Phys. Commun.* **60**, 165 (1990).
- [160] R. Mertig, M. Bohm, and A. Denner, *Comput. Phys. Commun.* **64**, 345 (1991).
- [161] T. Hahn and M. Perez-Victoria, *Comput. Phys. Commun.* **118**, 153 (1999), hep-ph/9807565.
- [162] K. Chetyrkin, J. Kühn, and M. Steinhauser, *Computer Physics Communications* **133**, 43 (2000), URL <https://doi.org/10.1016%2Fs0010-4655%2800%2900155-7>.
- [163] A. Buckley, J. Ferrando, S. Lloyd, K. Nordström, B. Page, M. Rüfenacht, M. Schönherr, and G. Watt, *Eur. Phys. J. C* **75**, 132 (2015), 1412.7420.
- [164] S. Dittmaier, *Nucl. Phys. B* **565**, 69 (2000), hep-ph/9904440.
- [165] Z. Nagy, *Phys. Rev. D* **68**, 094002 (2003), hep-ph/0307268.
- [166] Z. Nagy and Z. Trocsanyi, *Phys. Rev. D* **59**, 014020 (1999), [Erratum: *Phys.Rev.D* 62, 099902 (2000)], hep-ph/9806317.
- [167] R. Frederix, T. Gehrmann, and N. Greiner, *JHEP* **09**, 122 (2008), 0808.2128.
- [168] T. Gehrmann and N. Greiner, *JHEP* **12**, 050 (2010), 1011.0321.
- [169] R. L. Workman et al. (Particle Data Group), *PTEP* **2022**, 083C01 (2022).
- [170] R. D. Ball et al. (NNPDF), *Eur. Phys. J. C* **77**, 663 (2017), 1706.00428.

- [171] V. Bertone, S. Carrazza, N. P. Hartland, and J. Rojo (NNPDF), *SciPost Phys.* **5**, 008 (2018), 1712.07053.
- [172] R. D. Ball et al. (PDF4LHC Working Group), *J. Phys. G* **49**, 080501 (2022), 2203.05506.
- [173] S. Bailey, T. Cridge, L. A. Harland-Lang, A. D. Martin, and R. S. Thorne, *Eur. Phys. J. C* **81**, 341 (2021), 2012.04684.
- [174] T. Cridge, L. A. Harland-Lang, A. D. Martin, and R. S. Thorne, *Eur. Phys. J. C* **82**, 90 (2022), 2111.05357.
- [175] A. Manohar, P. Nason, G. P. Salam, and G. Zanderighi, *Phys. Rev. Lett.* **117**, 242002 (2016), 1607.04266.
- [176] A. V. Manohar, P. Nason, G. P. Salam, and G. Zanderighi, *JHEP* **12**, 046 (2017), 1708.01256.
- [177] G. Belanger, F. Boudjema, J. Fujimoto, T. Ishikawa, T. Kaneko, K. Kato, and Y. Shimizu, *Phys. Rept.* **430**, 117 (2006), hep-ph/0308080.
- [178] A. Sirlin, *Phys. Rev. D* **22**, 971 (1980).
- [179] A. Denner, *Fortsch. Phys.* **41**, 307 (1993), 0709.1075.